Exploratory morphodynamic hindcast of the evolution of the abandoned Yellow River delta, 1578-1855

Su, Min; Yao, Peng; Wang, Zhengbing ; Zhang, C.K.; Stive, Marcel

Important note
To cite this publication, please use the final published version (if applicable).
Please check the document version above.

Accepted Manuscript

Exploratory morphodynamic hindcast of the evolution of the abandoned Yellow River delta, 1578-1855 AD

Min Su, Peng Yao, Zheng Bing Wang, Chang Kuan Zhang, Marcel J.F. Stive

Please cite this article as: Su, Min, Yao, Peng, Wang, Zheng Bing, Zhang, Chang Kuan, Stive, Marcel J.F., Exploratory morphodynamic hindcast of the evolution of the abandoned Yellow River delta, 1578-1855 AD, *Marine Geology* (2016), doi: 10.1016/j.margeo.2016.11.007
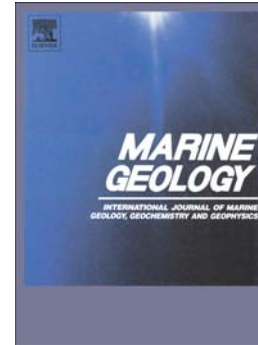
Exploratory morphodynamic hindcast of the evolution of the abandoned Yellow River delta, 1578-1855 AD

Min Su [a,b,c], Peng Yao [a,b,c,*], Zheng Bing Wang [b,d,e], Chang Kuan Zhang [e], Marcel J.F. Stive [b]

[a] *Institute of Estuarine and Coastal Research, School of Marine Sciences, Sun Yat-Sen University, No. 135, Xingang Xi Road, Guangzhou, 510275, China*

[b] *Faculty of Civil Engineering and Geosciences, Department of Hydraulic Engineering, Delft University of Technology, P.O. Box 5048, 2600 GA Delft, The Netherlands*

[c] *Guangdong Provincial Key Laboratory of Marine Resources and Coastal Engineering, Guangzhou 510275, China*

[d] *Deltares, Marine and Coastal Systems, P.O. Box 177, 2600 MH Delft, The Netherlands*

[e] *College of Harbor, Coastal and Offshore Engineering, Hohai University, 1st XiKang Road, 210098 Nanjing, China*

[*] *Corresponding author. Tel.: +86 756-3668259. Email address: yaop3@mail.sysu.edu.cn*

Abstract：

The Abandoned Yellow River Delta (AYD), which formed when the Yellow River flowed into the Southern Yellow Sea between 1128 and 1855 AD, is a representative example of the sensitivity of deltas to modifications in their environments. In this study, we established a process-based morphodynamic model to explore the morphological evolution of one such large-scale fine-grained delta (the AYD before 1855). The uncertainties in the model settings, which are inevitable when historical data are insufficient, were assessed together with the corresponding influences on the evolution of the deltaic system by considering a series of scenarios. The results indicate that the strength of local tidal forcing is the key factor that determines the shape and evolutionary trend of the delta. Sediment input discharge and the slope of the initial coastal profile have a considerable effect on the overall size of the delta and the relative ratio between subaerial and subaqueous parts of the delta, respectively. Based on the evaluation of the uncertainties and a comparison with historical maps, the simulated AYD was evaluated to be reliable. Through an analysis of the temporal delta evolution and residual sediment transport, the morphological evolution of the AYD before 1855 AD was investigated. The southern delta grew as the shoals merged with the mainland, which is in agreement with an existing hypothesis (Zhang, 1984), whereas the accretion of the northern delta was independent from the shoals in the northern part. Additionally, suggestions are made regarding the distribution of the AYD at the end of its progradation stage, which provides fundamental information for analyzing subsequent erosion processes since 1855 AD. This study differs from existing studies on the AYD, which are all based on geological approaches. It provides insight into the evolution of the AYD through an alternative means, viz. a process-based morphodynamic-modeling approach.

Key words: abandoned Yellow River Delta, morphodynamics, process-based modeling, uncertainty, historical maps

1. Introduction

A river delta can be formed when a river flows into a relatively larger water body (e.g., an ocean, lake, or gulf). The morphology of a delta is a dynamic balance between the fluvial discharge, marine energy conditions, accommodation space and overall geological setting (Wright and Coleman, 1973; Giosan, 2007; Hanebuth et al., 2012), with contributions from sea-level rise and human activities (Edmonds and Slingerland, 2009). Deltas are fragile geomorphic landscapes and can change dramatically with slightest modification to the aforementioned conditions (e.g., fluvial and marine hydrodynamics; Giosan, 2007). For example, the historical morphodynamic equilibrium (i.e., stable morphodynamic behavior; Guo, 2014) of river deltas (lobes) can be disturbed owing to the elimination of a fluvial sediment supply caused by river avulsion or by anthropological influence (Roberts, 1997; Jiménez et al., 1997; Syvitski and Saito, 2007; Frihy et al., 2008; Milliman et al., 2008, Gelfenbaum et al., 2009; Nienhuis et al., 2013). In particular, a delta becomes abandoned when river sediment input is no longer provided for the deltaic system. Compared with an active delta, an abandoned delta is mostly dominated by marine processes (e.g., tides and waves) (Woodroffe, 2003; Anthony, 2015).

Most of the well-studied abandoned deltas (lobes) worldwide are coarse grained (e.g., the Ebro delta lobe, Batalla et al., 2014; the Po delta, Stefani and Vincenzi, 2005) and/or wave dominated/influenced (Woodroffe and Saito, 2011). The morphological feature of those deltas (lobes) is the well-known beach barrier (or cheniers) system on a sandy (or muddy) substrate, e.g., the Chandeleur Islands in the Mississippi delta (Woodroffe and Saito, 2011; Anthony, 2015). Specifically, those existing studies mostly concentrated on wave impacts (e.g., Nienhuis et al., 2013; Anthony, 2015), the evolution of spits (e.g., Simeoni et al., 2007; Sabatier et al., 2009) and

4

whole delta evolution cycles (e.g., Coleman, 1998). Compared with those deltas, the abandoned Yellow River delta in the Yellow Sea is quite unique because it is fine grained and tidally dominated (Woodroffe and Saito, 2011). The Abandoned Yellow River (Huanghe) delta (AYD) was formed by the old Yellow River (OYR) from 1128 to 1855 AD (Xue, 1993) (Figures 1 and 2). It has undergone severe erosion since 1855 AD, when the Yellow River shifted its course to the Bohai Sea (Ren & Shi, 1986; Xue, 1993; Saito et al., 2000; Liu et al., 2013).

Under energetic hydrodynamics (e.g., tidal currents exceeding 1.5 m/s on the southern Jiangsu coast and exceeding 0.5 m/s on the northern Jiangsu coast; Liu et al., 2013) and abundant fluvial sediment from the OYR during 1128 and 1855 AD, the hydrodynamics, sedimentology and morphology in the western Southern Yellow Sea (SYS) were inevitably modified with the significant seaward accretion of the shoreline (Liu et al., 2013). For example, almost the whole Jiangsu Coast (Figure 1), i.e., from 34.2°N to 32.7°N, changed from a sandy beach to a silt-clayey coast in the period 1128-1855 (Liu et al., 2010; Xue et al., 2011). In addition, Ren and Shi (1986) stated that a considerable part of the well-known radial sand ridges in the SYS (Figure 1) is composed of the sediment from the OYR. Considerable efforts have been devoted to investigate the erosion process to forecast the fate of the abandoned delta. Many existing studies have investigated the morphological and hydrodynamic changes during the erosion stage of the AYD, e.g., the cross-shore profile changes (Zhang et al., 1998), estimating the overall volume of the erosion (Saito and Yang, 1995), the transport direction of eroded sediment (Ren and Shi, 1986; Saito and Yang, 1995; Shi et al., 2012; Zhou et al., 2014) and the feedback of erosion to the tidal dynamics (Chen et al., 2009). However, morphodynamics during delta progradation period have received little attention (Liu et al., 2013; Xia et al., 2015).

5

Studies of the morphodynamic evolution of the abandoned delta can deepen our understanding of the so-named "delta cycle" (Robert, 1997), because the abandoned delta can be considered as a natural, 1:1 scale "laboratory" study case. The reconstruction of the AYD morphodynamics (fine grained and tidally dominated) is expected to inspire geologists and coastal scientists to advance the understanding of some recent deltas that differ from the mainstream (i.e., coarse grained and/or wave-dominated/influenced abandoned deltas and lobes). Similarly, Geleynse et al. (2011) stated that a good understanding of the present state of deltas is required to understand their future dynamics. Enriching our understanding of the evolution before abandonment, such as the mechanisms governing morphodynamics, spatial distribution of sediment and the size of the deltaic system, benefits the understanding of the subsequent erosion processes. However, studies seeking to understand the sedimentary characteristics of the progradation of the AYD have been qualified as superficial (Liu et al., 2013). On the one hand, the applied methodologies are limited to geological and geophysical approaches that include sedimentological, mineralogical and geochemical methods (Yang et al. 2003). On the other hand, the objectives of existing studies focus on speculations on the spatial distribution of the AYD (Liu et al. 2013). Unfortunately, the results of the spatial distribution of the AYD are inconsistent with each other and are even considered to be controversial (more details are provided in section 2.2). This may be partly due to the inherent restrictions of geological approaches (e.g., core drilling and seismic profiles), which commonly focus on the sedimentary record rather than on the recovery of historical events, including erosion. Therefore, an alternative approach is suggested to improve the understanding of the progradation process of the AYD.

Long-term morphodynamic modeling is a useful tool to explore the formation and governing mechanisms of morphological patterns such as deltas, estuaries and other coastal systems (De

Vriend et al., 1993, Stive and Wang, 2003; Roelvink and Reniers, 2011; Coco et al., 2013; Guo et al., 2015). Moreover, process-based models have been examined as a promising and perspective approach for long-term modeling (Jiménez and Arcilla, 2004; Dissanayake and Roelvink, 2007; Karunarathna et al., 2008). To avoid time consuming computations, "input reduction" concepts and morphological acceleration techniques have been implemented in models (Cayocca, 2001; Wu et al., 2007; Dastgheib et al., 2008). Techniques that reduce complexity are commonly applied, especially for deltas, which are sensitive to many influencing factors. For example, a model of a river-dominated delta was developed to explore the relationship between the distributary channel and river discharge and sediment cohesiveness (Edmonds and Slingerland, 2010; Edmonds et al., 2010). Similarly, Geleynse et al. (2010) investigated the formation of detailed deltaic system features (e.g., distributary channels) and stratigraphy, considering river discharge only and ignoring tides and waves. Subsequently, Geleynse et al. (2011) improved the numerical delta scheme by combining the influences of river, tides and wind waves to assess the influence of wind-generated waves and tides on delta formation. Guo et al. (2015) adopted a schematized 2D fluvio-deltaic morphodynamic model (representing the Yangtze River Estuary), which was forced by river flow and tides, to assess morphodynamic sensitivities to river discharge magnitude and seasonal variations.

The purpose of this study is to document the natural evolution of the progradation process of the AYD, with particular focus on a hindcast of the depositional process of sediment, taking into account several uncertain conditions. Owing to data scarcity, we combined several available complementary sources of information in this study. (1) Historical records and maps drawn during the delta progradation period are presented to offer a general impression on the progradation of the AYD and the evolution of the adjacent Jiangsu Coast. Prominent events of

the OYR are reviewed, and major evolutionary features of the AYD are deduced. In addition, geological evidence for discriminating the delta range and estimating the delta size is reviewed. (2) Reduced complexity numerical models can be used to efficiently investigate long-term morphodynamics (Seybold et al., 2009; Geleynse et al., 2010). Therefore, to interpret the morphological evolutionary process of the AYD during past centuries, we constructed a process-based morphodynamic model. (3) Because a delta is a dynamic large-scale terrestrial-oceanic system (Swenson, 2005), changes in any of the uncertainties in that system can alter the overall distribution of sediment and delta morphology (Gelfenbaum et al., 2009). Thus, uncertainties in the model parameter settings owing to scarce historical data critically impact hindcasting the evolution of the deltaic system. Therefore, a series of scenarios was designed with various settings of uncertain parameters to hindcast the consequent distribution of the AYD. (4) The model results are presented as maps. Subsequently, the reliability of model results and their uncertainties are assessed based on a comparison with the historical maps and results of geological studies.

Figure 1. Map of the study area (inside the dotted rectangular) with 20-m and 50-m isobaths in the Yellow Sea. The reference shoreline of the Jiangsu Coast in 1128 AD was modified after Yang et al. (2003) and Gao (2009). The location of the OYR was modified after Lim et al. (2007) and Liu et al. (2013). Colored regions A and B represent the approximate locations of the AYD and radial sand ridge field, respectively (modified after Park et al., 2000).

2. Study area, data and methods

2.1 General information

The Yellow Sea, which is located between the Chinese mainland and the Korean Peninsula, is divided into the Northern Yellow Sea sector (NYS) and the Southern Yellow Sea sector (SYS) according to their geographical positions relative to the Shandong Peninsula (Figure 1) (Wang and Aubrey, 1987). The SYS, which is located between the Shandong Peninsula and the East China Sea, has an area of over 300,000 km^2 and an average depth of 45 m. Tides are a major force in this area, especially the semidiurnal tide (Liu et al., 2013). The tidal amplitude of the M2 constituent is approximately 1 - 2 m along the Jiangsu Coast (Yang et al., 2003; Su et al., 2015). The western part of the SYS is dominated by a strong tidal current (i.e., the maximum velocity reaches 1.4 m/s; Teague et al., 1998), with convergent-divergent tidal currents in the radial sand ridge area and north-south along-shore currents around the AYD (Zhu and Chang, 2000; Yang et al., 2003).

The Yellow River, which discharges into the Bohai Sea at present (Figure 1), is well-known for the large amount of silt it carries (Tregear, 1965; Van Maren et al., 2009). Although it has a modest freshwater discharge (4.9×10^{10} m^3/y), it carries the second largest sediment load in the world, which is estimated to be 1.2×10^9 t/y, that reaches the ocean (according to data observed between 1950 and 1970; Milliman et al., 1987; Wang and Aubrey, 1987; Liu et al., 2013). Its course alternated northward and southward frequently and unexpectedly during the historical time period described below (Figure 2). The last time it shifted southward and discharged into the SYS occurred from 1128 to 1855 AD.

9

According to historical documents, four historical phases during the evolution of the AYD can be distinguished. (1) 1128-1494 AD. In 1128, an artificial distributary channel was excavated for a military strategic reason, and approximately 60%~80% of the total discharge of the OYR occupied the Huai River (Huaihe) channel into the SYS at the Jiangsu Coast (Zhang, 1984; Zhou et al., 2014). River-course shifts and crevasses frequently occurred from 1128 to 1494 AD, resulting in large deposits in the lower flood plain and fluvial plain rather than contributing to delta seaward progradation (Ye, 1986; Li, 1991; Liu et al., 2013; Zhou et al., 2014). (2) 1495-1577 AD. After 1495 AD, the OYR discharged exclusively into the SYS owing to anthropogenic embankments (Ye, 1986; Milliman et al., 1987; Li, 1991; Liu et al., 2013). (3) 1578-1855 AD. Another remarkable anthropogenic influence on the evolution of the OYR and AYD is a well-known river-training project based on a strategy to "concentrate the current to attack the silt" (Ye, 1986; Li, 1991; Xue et al., 2011; Zhang et al., 2014; Chen et al., 2015). It began to impact the evolution of the AYD after 1578 AD, and sediment began to deposit, primarily at the river mouth. Its effect lasted for the following hundreds of years until 1855 AD. (4) 1855 AD. In 1855, a significant breach changed the river course (Ye, 1986; Xue, 1993; Syvitski and Saito, 2007; Zhou et al., 2014). An abrupt cessation of sediment supply to the delta resulted in severe erosion of the delta (Wang and Aubrey, 1987).

Generally, during the time period 1128-1855 AD, anthropogenic influences are implied to have significantly impacted the lower Yellow River (Chen et al., 2015). The sediment loads, position of river mouth, river management strategy and the shifting river course were all affected by humans (Wang and Aubrey, 1987; Zhang et al., 2014). Eventually, the morphological evolution of the AYD was greatly influenced. In particular, since 1578 AD, the channel of the OYR has

been almost fixed, and the deltaic progradation rate increased dramatically as a result of human embankments and channel training (Xue et al., 2011; Chen et al., 2015).

Figure 2. Shift in the course of the Yellow River (modified after Tregear, 1965; Wang and Aubrey, 1987 and Zhang et al., 1998). For more details on river course shifts, including small distributaries, see Liu et al. (2013).

Historical maps offer a pictorial impression of the Jiangsu Coast and AYD. In this study, several ancient maps were collected to interpret the progradation of the delta (see the Appendix). Considering the purpose of the historical maps, i.e., primarily as a tool for the government allocation of land, collecting taxes, defense and design of cities and management of farmland irrigation, and because of the restriction imposed by measurement instruments in those early ages, most historical maps were not constructed with a recognizable coordinate system (e.g., longitude and latitude coordinates). To take advantage of the historical maps for scientific research, efforts have been made to reference them to the longitude and latitude system (e.g., Zhang, 1984), and the adjusted shorelines have been shown in the recent literature (e.g., Gao, 2009; Zhou et al., 2014). Adding coordinates to historical maps does benefit scientific study, but it must be remembered that the geometrical accuracy of the results may not be as high as expected. Nevertheless, if employing original historical maps as conceptual maps, the derived qualitative results are relatively credible. Two features of the Jiangsu Coast summarized from historical maps during 1578 and 1855 AD are remarkable. (1) A significant geometrical feature of the Jiangsu Coast was a previously dense channel network, and the region with a dense channel network was subsequently reduced over time. (2) Numerous shoals were generated along the Jiangsu Coast over time (see the Appendix). Although the shoals are shown with different shapes, the existence and general location of the shoals are similar.

2.2 Spatial distribution of the AYD

A deltaic system may be distinguished in the subaqueous delta and subaerial delta, which are defined traditionally according to their relative positions with respect to mean sea level (Wright and Coleman, 1974). Simultaneous with the progradation of the subaerial delta, a huge subaqueous delta was formed (Ren and Shi, 1986; Li et al., 2001; Yang et al., 2002; Liu et al., 2013). For example, it has been reported that the size of the modern Yellow River delta plain extended more than 5710 km^2 into the Bohai Sea within 150 years (i.e., 1855-2005) (Syvitski and Saito, 2007). However, the marine hydrodynamics (e.g., tidal range) and local bathymetries (e.g., cross-shore slope) are different for the modern Yellow River delta and AYD (Ren, 1987; Zhang et al., 2012).

In recent decades, the geographical features of the AYD have been studied using geochronological data and drilling, seismic, stratigraphic, sedimentological and geochemical surveys (e.g., Liu et al., 2012, 2013; Wang et al., 2012). The obtained understandings of the scope and size of the delta are controversial (Xia et al., 2015). There are dozens of viewpoints on the spatial distributions of the subaerial and subaqueous deltas. The detailed and controversial estimates of the subaerial delta in terms of their alongshore lengths and sizes are shown in Table 1 and Figure 3a, and those of the subaqueous delta are shown in Table 2 and Figure 3b. Note that the literature on the distribution of the subaerial delta does not document the detailed distribution boundary but only highlights the northernmost and southernmost boundaries.

Figure 3 shows that the uncertainties in the locations of the northern boundaries of the subaerial and subaqueous deltas are relatively small. The major controversies focus on the determination of the southern and the eastern boundaries of the delta. Estimates for the southern boundary of the

delta vary from 33°50′N (Sheyang Estuary) to 32°35′N (near Yangkou), a difference of greater

than 144 km (Figures 3a, b). In addition, the estimated eastern boundary of the subaqueous delta

ranges from 121°E to almost 123°E, with a greater than 180 km difference (Figure 3b). The

uncertainties in the southern and eastern boundaries may be due to the lack of sufficient surveys.

The existing surveys mainly focused on the region near the river mouth rather than covering the

total estimated scope (e.g., Yuan and Chen, 1984; Liu et al., 2013). Moreover, the estimated

shape of the subaqueous delta is quite different (Figure 3b) and includes a symmetric fan shape

(e.g., viewpoint ⑫), an asymmetric fan shape (e.g., viewpoint ②), a lateral elongate asymmetric

shape (e.g., viewpoint ⑩) and a longitudinal elongate asymmetric shape (e.g., viewpoint ⑨). To

date, the accuracy and consistency of the scope and size of the AYD obtained by the geological

approaches is considered to be quite poor (Liu et al., 2013).

Table 1. Estimates of the size of the subaerial delta of the AYD developed during the years 1128-1855 AD.

Table 2. Estimates of the size of the subaqueous delta of the AYD developed during the years 1128-1855 AD.

Figure 3. Overview of viewpoints on the spatial distributions of the subaerial delta and the subaqueous delta (modified after Liu et al., 2013 and Xia et al., 2015). The numbers are consistent with those in Tables 1 and 2.

2.3 Morphodynamic modeling

2.3.1 Model description

A long-term process-based 2DH morphodynamic model developed using Delft3D software was

set up to simulate the dynamic progradation process of the delta and to reconstruct the AYD.

Unlike the geological point of view, the focus of the process-based morphodynamic model is the

coupling of physical processes, including hydrodynamics, sediment transport and bed morphology.

Delft3D solves the unsteady shallow-water equations in two/three dimensions. Sediment transport and morphological changes are computed simultaneously with the flow. It can simulate hydrodynamic and morphological changes at timescales from seconds to thousands of years by using a representative hydrodynamic setting and a morphological acceleration factor (De Vriend et al., 1993; Roelvink, 2006; Dastgheib et al., 2008). Validation of the basic sediment transport and morphology updating model were reported in Lesser et al. (2004) and Ranasinghe et al. (2011). Delft3D has been successfully applied in a range of fluvial and coastal environments to study nearshore morphology such as the evolution of rivers and deltas (e.g., Edmonds and Slingerland, 2009; Caldwell and Edmonds, 2014). In addition, it has been applied to model high sediment concentrations in the modern Yellow River (van Maren et al., 2009). We implemented this process-based model, with reduced complexity, in an attempt to gain insight into the progradation of the AYD.

(1) Hindcasting time frame

Owing to the significant anthropogenic influences on the OYR, the hindcasting time frame should be cautiously selected to match the distinct historical phases. For example, the progradation rate of the delta before 1578 AD was relatively small because of the frequently shifting river course (Li, 1991). The river course was less active after 1578 AD because of a river training project, which resulted in a rapid progradation of the delta (Zhou et al., 2014). Therefore, the period from 1578 to 1855 AD was selected as the hindcasting period.

(2) Model domain and grids

The model domain covers the western part of the SYS, which is located between the Shandong Peninsula and the Yangtze River Estuary (Figure 4a). Considering the geological estimation of the possible distribution of the AYD (Figure 3), a large-scale domain is required for simulating a large-scale delta. To be consistent with the simulation time frame, the reference Jiangsu shoreline of 1578 AD was taken as the western land boundary. The eastern and southern boundaries were set to open boundaries (Figure 4a). To enhance the computational efficiency for a morphological simulation that covered almost 300 years and extended over a large-scale domain and to highlight the simulation accuracy around the river mouth, the model was decomposed into three sub-domains (see 'Domain Decomposition Technique' in Deltares, 2012 for more details) (Figure 4a). Domain decomposition is efficient for nesting models with different grid scales (Smith et al., 2004), and its feasibility for morphological simulations has been demonstrated by previous studies (e.g., Luijendijk et al., 2004; Yossef et al., 2008; Ruggiero et al., 2009; Nguyen et al., 2010). In each sub-domain, curvilinear grids were created under spherical coordinates (Figure 4b). The grid resolution varied from 279 m to 3190 m, with adequate spatial resolution in the vicinity of the river mouth.

Figure 4. Domain and grid of the morphological model. (*a*) Configuration of the land boundaries (red lines) and open boundaries (blue lines). The land boundary near the Jiangsu Coast is the reference shoreline of 1578 AD (modified after Gao, 2009). The black dotted lines denote the shoreline at present. The three sub-domains divided by the orange lines are designated I, II and III. (*b*) Enlarged grids of the adjacent sub-domains at regions A and C (different sub-domains use different colors), with an enlarged figure for the river boundary (B). The sub-domain II grid has a relatively higher resolution (~ 279 m × 375 m). (*c*) Longitudinal profile of the initial bathymetry near the river mouth (green lines in panel (*a*)).

(3) Initial bathymetry

Owing to the lack of historical data, the initial bathymetry for the model was constructed schematically based on the mean water depth at present in the SYS (~45 m), taking into account the estimated total sediment volume carried by the OYR into the SYS since 1578 AD, which is approximately 2~3.9×10^8 t/y (e.g., Li, 1991; Zhang et al., 2014) and the mean sea level rise (~2 mm/year; State Oceanic Administration, 2003). Furthermore, the nearshore bathymetries were optimized by analyzing sedimentary data from several publications (e.g., Ye, 1986; Li, 1991; Yang et al., 2002). The bathymetry around the radial sand ridges was determined considering that the distributary channels of the ancient Yangtze (Changjiang) River underlay the southern part of sand ridges (Wang et al., 2012). The overall configuration of the initial bathymetry is shown in Figure 6a. The bed slope of the SYS near the river mouth was set to ~0.175‰ (Figure 4c), according to a schematized 2D numerical model for the Jiangsu coast (i.e., 0.16‰~0.46‰; Zhu and Chang, 2001). The hydraulic roughness was considered using a constant Manning coefficient with a value of 0.016, based on modeling experiences in the SYS (Su et al., 2015). The time step of the flow computation was 60 s for reasons of accuracy and stability.

(4) Hydrodynamics

Local hydrodynamics such as tides, waves and alongshore currents are responsible for the delta morphology and nearshore bathymetry development (Orton and Reading, 1993; Liu et al., 2013). However, no measurements are available for the period 1578 − 1855 AD (Syvitski and Saito, 2007). Among marine dynamics, tides, particularly the M2 constituent, are the most dominant factor in the study area (Zhu and Chang, 2000). In addition, the tidal force has been demonstrated to have been stable over the past thousands of years (Zhu, 1998; Uehara et al., 2002; Wang et al., 2012), compared with other uncertain hydrodynamic forces (e.g., wave and wind). Thus, tides were the only hydrodynamic force considered in the model. The M2 tidal constituent, which is

the primary tidal component in the SYS, was prescribed along the open boundaries. The phases and amplitudes of the M2 tidal constituent were extracted from a well-calibrated present-day tidal wave model that covers the Bohai Sea, Yellow Sea and East China Sea (Su et al., 2015).

With respect to the river boundary, only the data for the modern Yellow River can provide some inspiration for the determination of the OYR river discharge. The multi-year averaged discharge of the modern Yellow River is 1630 m^3/s. Floods frequently occurred in the historical time period (Chen et al., 2015), and floods lead to high concentrated flows (Wang and Xu, 1999; Li et al., 2014). We admit that the process of river discharge is unsteady (e.g., floods). However, to enhance the computational efficiency given long-term morphological changes, we set the feeding river discharge of the OYR in the model to a constant value and ignored the increased water and sediment discharges during floods. According to a series of preliminary calibrations (not shown here), we set the water discharge in the model to 2550 m^3/s.

(5) Sediment transport

It has been reported that almost 80% of the Jiangsu Coast was sandy before the OYR flowed into the SYS (Xue et al., 2011). Therefore, the bottom sediment of the SYS was set to sand with a uniform grain size of 200 μm, and spatial variations were ignored. The multi-year averaged median grain size of the modern Yellow River is 19 μm (Chinese Ministry of Water Resources, 2011). Gao et al. (1989) and Chen et al. (2015) recommended that the median grain size for historical periods was slightly smaller (~15 μm). Therefore, the size of the sediment carried by the OYR was set to 15 μm in the model, with a settling velocity of 0.2 mm/s.

Non-cohesive sediment transport was calculated following Van Rijn (1993) formulations. Cohesive sediment transport was calculated following Partheniades-Krone formulations (Partheniades, 1965):

$$E = M(\frac{\tau_b - \tau_{cr,E}}{\tau_{cr,E}}), \quad \tau_b > \tau_{cr,E}$$

$$D = \omega_s c(\frac{\tau_{cr,D} - \tau_b}{\tau_{cr,D}}), \quad \tau_b < \tau_{cr,D}$$

in which, E and D are erosion/deposition fluxes (kg/m^{2}s); M is an erosion parameter (kg/m^{2}s); τ_b is the maximum bed shear stress (N/m^2); $\tau_{cr,E}$ and $\tau_{cr,D}$ are the critical erosion/deposition shear stress (N/m^2) (When $\tau_b < \tau_{cr,E}$, $E = 0$; when $\tau_b > \tau_{cr,D}$, $D = 0$); c is the sediment concentration (kg/m^3). Hindered settling effects were considered in the model with the Richardon-Zaki equations as $\omega_s = \omega_0(1 - \phi)^n$, in which ω_0 is the particle settling velocity in clear water and ω_s is the particle fall velocity under the volumetric sediment concentration ϕ. More details can be found in Delft3D manual and van Maren et al. (2009). The simulated sediment fluxes as well as the local bed morphology depend on the relationship between deposition (D) and erosion (E), which further depend on $\tau_{cr,E}$, $\tau_{cr,D}$, c and M. The existence of $\tau_{cr,D}$ is debated (Edmonds and Slingerland, 2009): sedimentation can occur simultaneously with erosion (Winterwerp, 2006), or not (Maa et al., 2008). Van Maren et al. (2009) argued that sedimentation never happens for hyperconcentrated flow (over 200 kg/m^3). Besides, he recommended that it is comparable to either use a smaller $\tau_{cr,D}$ or use a larger M. Thus, with a consideration of the depth-averaged sediment concentration of the OYR considered in the model (i.e., not the hyperconcentrated flow), we choosed to tune parameter M to make the simulations realistic. In this study, $\tau_{cr,E}$ and $\tau_{cr,D}$ were set to be 0.5 N/m^2 and 1000 N/m^2, indicating sedimentation occurs

18

constantly. The erosion parameter M was set as 0.01 kg/m^{2}s. Additional experiments (not shown here) demonstrated that, if smaller erosion parameters were applied to the model, severe sedimentation would occur along the river channel, resulting in a filled-up, and even, blocked channel. When larger erosion parameters were assigned, the progradation ratio of the AYD was decreased. And, eventually the simulations would not catch the protuberance feature near the river mouth, which is inconsistent with the records in the literature (e.g., Zhang, 1984; Ye, 1986; Liu et al., 2013).

The sediment supply at the upstream river boundary was determined based on the annual sediment load transported into the SYS by the OYR. It has been predicted by several previous studies, although the estimates vary greatly. For example, Zhang et al. (2014), Li (1991), Huang et al. (2005) and Ren (2006) estimated that the annual sediment amount was 2×10^8 t/y, $2.5\sim3.9\times10^8$ t/y, 5×10^8 t/y and 6×10^8 t/y, respectively. In this study, the sediment concentration was set to 3 kg/m^3, yielding an annual averaged sediment load of 2.4×10^8 t/y. The sand fluxes were given by a zero concentration gradient at the offshore open boundaries. Thus, the bed level at the open boundaries was constant.

A spin-up period of 720 minutes without morphological updating allowed the flow to stabilize. Based on a series of preliminary sensitivity experiments, an acceleration factor of 108 was used. The morphological change at each time step was multiplied by the carefully selected acceleration factor (Roelvink, 2006) to appropriately accelerate the evolution and make the long-term simulation more efficient (Dissanayake et al., 2009). In this study, the drying and flooding processes were defined using a threshold depth of 0.1 m. A dry cell erosion approach, which is preferable for simulating channel migration, was not considered in the present study. Ignoring dry cell erosion helped us prevent frequent course shifting of the OYR, which is consistent with the

contribution of artificial riverbanks since 1578 (mentioned in section 2.1). Detailed processes relating sand-mud interactions were not implemented. In the model, the OYR-derived sediment (15 μm) was simulated to deposit above the layer of the sand fraction (200 μm). Therefore, the erosion rate of the finer sediment was not reduced. This simplification was reasonable for the long-term and large-scale morphodynamic modeling in this study.

2.3.2 Specification of model scenarios

To explore the effect of the uncertainties, a series of scenarios was designed. The simulation presented in section 2.3.1 was taken as a reference run. Various scenarios were designed based on the reference run, considering one uncertain parameter in each scenario while holding the other parameters unchanged.

Bathymetric data, sediment discharge and river discharge have been reported to determine the progradation ratio of a deltaic system (Wright and Coleman, 1973; Orton and Reading, 1993; Gelfenbaum et al., 2009; Kleinhans et al., 2010). Specifically, with respect to the modern Yellow River Delta, the ratio between the sediment concentration (c) and water discharge (q) was proposed to be important (Li et al., 2001; Hu and Cao, 2003). However, these important parameters are uncertain for simulating the progradation of the AYD. The uncertainty in the initial bathymetry was examined by varying the initial bed slopes, with $\pm 10\%$ deviations from the slope in the reference run (cases BL and BH in Table 3). The possibility of other estimated volumes of sediment supply (mentioned in section 2.3.1) was applied to evaluate the influence of sediment availability (cases SL and SH in Table 3). By varying the water discharge and sediment concentration while keeping the total sediment supply constant, a relatively larger c/q (i.e., ~1.5

times larger) was applied in case WS. The water discharge (q) in case WS equaled the multi-year averaged discharge of the modern Yellow River (i.e., 1630 m³/s).

In the reference run, the temporally varying sediment discharge from the river was simplified to a constant during the 277 simulation years. It was worthwhile to assess whether a significant change of final morphologies could be caused by this simplification (case VV in Table 3). In addition, although tidal conditions were not taken to be uncertain in this study, different distribution features of the modern Yellow River delta (the local M2 tide amplitude is 0.2~0.4 m) and the AYD (the local M2 tide amplitude is 0.6~1 m) inspired us to discuss the contribution of the tidal regime on the evolution of a fine-sediment delta (cases WL and WH in Table 3).

Table 3. Applied sensitivity parameters for different scenarios.

3. Model results

3.1 Model results for the AYD

3.1.1 Hydrodynamics along the Jiangsu Coast

The simulated co-tidal chart and tidal current ellipses corresponding to the initial bathymetry (reference run) are shown in Figure 5. In comparison with the Marine Atlas of the Bohai Sea, the Yellow Sea, and the East China Sea (Atlas of the Oceans Editorial Board, 1993), the tidal wave propagation of the M2 constituent was similar to the present situation, as Uehara et al. (2002) argued. For example, an amphidromic point extending from the OYR river mouth and a converged tidal wave near the radial sand ridge area were both well modeled (Figure 5a). The tidal ellipses of the Jiangsu Coast indicated two remarkable tidal current patterns: a rectilinear

current along the northern Jiangsu Coast (especially near the OYR) and a radial current pattern surrounding the southern Jiangsu Coast (Figure 5b). In addition, the local tidal currents were relatively strong and exceeded 1 m/s. Rotating tidal currents were found at the northernmost and southernmost of the Jiangsu Coast. However, the direction of rotation was counter-clockwise in the northern part but clockwise in the southern part. The tidal current strengths at those two parts also varied. The tidal current magnitude of the southern rotating current was much (approximately three times) larger than the northern one (Figure 5b).

Figure 5. The simulated co-tidal chart (a) and tidal ellipses (b) of the M2 constituent near the Jiangsu Coast.

3.1.2 Morphological evolution

The sediment cohesiveness was demonstrated to control the pattern of the deltas (Edmonds and Slingerland, 2009). Under river discharge only and without marine forcing, the delta changes from a fan-shape to a bird's-foot shape with an increase in cohesiveness (Edmonds and Slingerland, 2009). The local hydrodynamics, especially along the Jiangsu Coast, are recognized to be energetic (Figure 5). The evolution of the AYD, which is formed by fine-grained sediments under energetic tidal currents, is suggested to differ from the results of Edmonds and Slingerland (2009). A recognized hypothesis for the evolutionary trend of the AYD has been proposed by Zhang (1984), who suggested that delta progradation occurred through the migration of nearshore shoals gradually towards the mainland. It is difficult to validate this hypothesis using geological observations, whereas a process-based morphodynamic model can elaborately describe the temporal evolution process of the delta and be used to examine the hypothesis.

Figure 6 shows the simulated temporal morphological evolution of the AYD. A remarkable feature is the large area of sedimentation along the Jiangsu Coast, with a protuberance near the river mouth. To clearly describe the delta progradation process, the delta was divided into southern and northern sections according to their geographic positions relative to the extension direction of the river channel. After 50 years in the simulation, a fluvial delta emerged around the river mouth (Figure 6b). The simulation indicates that the delta is characterized by an asymmetric distribution in the north and south directions, and the southern delta was much more developed. During the next 50 years, both the northern and southern deltas expanded gradually towards the sea (Figure 6c). Along the Jiangsu Coast, the protuberance at the river mouth was extraordinarily obvious, which indicates that the progradation rate was faster near the river mouth than along the adjacent regions. In addition, several patterns of shoals occurred near the river mouth. With continuous sediment input, the nearshore shoals, which were located both north and south of the delta, gradually grew and built up in the following 50 years (Figure 6d). Afterward, those developed shoals began to merge with the main delta, leading to the expansion of the subaerial delta (Figure 6e). At the same time, the tidal channels located inside the delta were eroding. In the following decades until 1855 AD (Figure 6f), offshore shoals outside the northern delta were under strong development and gradually built up outside the river mouth. Simultaneously, the southern part of the delta continued to migrate seaward, and large shoals developed.

Figure 6. Temporal evolution of the AYD. (a) ~ (f) show the initial morphology (1578 AD) and the morphological evolution after 50 y, 100 y, 150 y, 200 y and 277 y (1855 AD), respectively.

Based on the analysis of the temporal evolution of the AYD, the progradation mechanisms for the northern delta and the southern delta were shown to be different. For the southern delta, the

growth mainly occurred by the merging of the nearshore shoals, as suggested by Zhang (1984).

The shoals grew with the continuous sediment supply, which resulted in narrowing channels.

Consequently, the simulation exhibits the phenomena whereby the southern coastline to gradually

prograde seaward. Simultaneously, new shoals were formed, and the fates of the new shoals were

similar as long as the sediment supply was continuous. However, the evolution of the northern

delta was the result of the growth of several independent shoals, which grew separately and did

not tend to merge together (Figure 6). The channels among the shoals separated the shoals into

individual features. The empirical hypothesis suggested by Zhang (1984) captures the

evolutionary mechanism of the southern delta, but it is hard to comprehensively represent the

formation mechanism of the northern delta.

3.1.3 Residual sediment transport

Owing to the rapid progradation of the AYD, the overall sediment transport pattern has varied

throughout the whole period of morphological evolution. In this section, two time points during

the evolution period are taken as an example to investigate the temporal changes in sediment

transport. The residual sediment transport was calculated by integrating the instantaneous tidal

induced sediment transport over the duration of fourteen M2 tidal cycles (output frequency of 1

hour). Figure 7 shows the residual sediment transport patterns after simulation for 100 years and

200 years. After simulating 100 years, large volumes of sediment were mainly concentrated

outside the southern delta, with a relatively small portion outside the northern delta (Figure 7a).

For the southern part, the main transport direction of residual sediment transport was southward

along the shoreline. Specifically, a portion of residual sediment around the southernmost region

of a newly generated subaerial delta was transported landward, resulting in significant

sedimentation and a rapid expansion of the southern delta. Different features were observed for

24

the northern part, where the active sediment region was rather small compared to the southern part (Figure 7a). In addition, the residual sediment transport was first directed northward, along the shoreline, and then turned landward, forming a counter-clockwise circulation. The different features of sediment transport in the northern and southern parts can explain the different patterns of the northern and southern delta (Figure 6c). On the other hand, the residual sediment transport could receive feedback from morphological changes (e.g., submerged shoals), which can be recognized by the complicated transport directions in the yellow rectangular region in Figure 7a.

The distribution patterns of the residual sediment transport in the southern and northern directions after 200-year simulation did not show the asymmetric feature seen 100 years earlier (Figure 7b). Both the magnitude and the distribution extension near the northern part significantly increased. The extension of the northern part was mostly seaward, although the counter-clockwise sediment transport circulation still pointed towards land and prevented the sediment from being transported northward. The counter-clockwise transport, on the other hand, favored the formation and growth of offshore shoals (Figures 6e, f). The sediment transport direction near the southern delta was not landward as in the previous 100 years, but occurred at a certain angle. Thus, instead of a rapid seaward expansion, the southern delta continued to prograde seaward and southward at a moderate speed.

Figure 7. Residual sediment transport along the AYD after 100 (a) and 200 (b) simulation years. The magnitudes are in units of m^3/sm. The directions are shown by white arrows. The transport directions of the large magnitude regions are highlighted by red arrows.

The region with the largest residual sediment transport along the Jiangsu Coast was represented as an 'L' type pattern after simulation for 100 years (Figure 7a). The width of the distribution of

the residual sediment transport magnitude considerably increased in the southernmost region. However, an opposite, 'Γ', pattern appeared after 200 years of simulation (Figure 7b). The widest region of large magnitude of residual sediment transport moved to the northernmost region. This indicates that the shoals located in the northern part were in a rapidly growing stage. The conversion of the distribution pattern implies that the progradation emphasis of the deltaic system changed from a significant expansion of the southern delta to the development of shoals in the northern delta.

3.1.4 Distribution of sedimentation (OYR-derived sediment)

An understanding of the extent of the morphological influence of the OYR-derived sediment before the abrupt cessation of sediment supply (i.e., before 1855 AD) is important, because the extent of sedimentation provides crucial and fundamental information for the erosion stage of the AYD (after 1855 AD). However, field data obtained by geological methods such as drill cores are insufficient to provide comprehensive insight. Note that, because of the continuous severe erosion of the delta after 1855 AD, the distribution of sedimentation (especially derived by the OYR) has undergone significant changes. Geological techniques alone cannot be relied on to gain a deep understanding of the evolution of the AYD. Appling a multidiscipline approach is beneficial for a substantial and comprehensive understanding. Ren et al. (1994) estimated that the distributed area of the OYR-derived sediment ranged from Lianyungang in the north to nearly Yangkou in the south, which exceeds the scope of the subaqueous delta. However, no direct or proper evidence supports that statement.

Figure 8. Map showing the simulated depositional distribution of the OYR-derived sediment. Zones I, II and III were divided according to their positions relative to the OYR (separated by lateral light gray lines). The black lines denote the range over which the sediment carried by the OYR can influence the local morphology, according to a discriminate criterion of accumulated depositional thickness > 10 cm. The outline of the accumulated depositional thickness > 3 m is represented by the red dotted lines.

Figure 8 shows the deposited thickness distribution of the OYR-derived sediment after the 277-year simulation (for 1855 AD). In this study, a depositional thickness larger than 10 cm was taken as a criterion to discriminate the scope of influence of the sediment derived by the OYR (Figure 8). Similar to the distribution of the delta, the distribution of sedimentation was characterized by asymmetry. Most of the sediment was deposited in zone I, accounting for ~63% of total sediment volume, and the maximum deposition thickness exceeded 30 m. The averaged depositional thickness for zones II and III was approximately 1.4 m and 0.5 m, respectively. The sedimentation reached as far as ~230 km south of the river mouth, and ~76 km north of the river mouth. The seaward boundary was mostly parallel with the land boundary and was ~63 km away from the river mouth.

The thickness of subaqueous part of the AYD was investigated to be less than 3 m (Li, 1991). An accumulated depositional depth of 3 m is also shown in Figure 8, denoting a 'quasi-subaqueous' delta. By comparing the boundaries of the 3-m deposition region and the 10-cm deposition region, considerable deviations occurred at the southern SYS. This implies that the influence of OYR-derived sediment on the evolution of radial sand ridges field was not significant during the propagation of the AYD before 1855 AD. The main effect of the OYR-derived sediment was the progradation of the deltaic system.

3.2 Contribution of uncertainty to delta evolution

3.2.1 Pattern of the deltaic system

Figure 9 shows the sensitivity of the uncertainties on the morphological evolution of the delta. The qualitative comparison of the AYD's distribution pattern between the scenarios and the reference run (Figure 9a) is discussed in this section.

The effect of the bed slope of the initial bathymetry was assessed using cases BL and BH (Figures 9b, c). Compared with the reference run, the location of the subaqueous delta relative to the subaerial delta significantly changed. In the reference run, the subaqueous delta was distributed around the subaerial delta. However, it changed to the northeast of the subaerial delta when the initial bathymetry became gentler. When the initial slope was steeper, the subaqueous delta was located in the deeper water off the eastern edge of the subaerial delta. In addition, the development and location of the shoals were greatly influenced by the initial bed slope, based on the comparisons of the depositional thickness of the sediment (Figure 10). The comparisons indicate that a gentler slope promotes the generation of more merged shoals nearshore. The response of the deltaic system may be because a gentle topography favorably attracts the nearshore deposition of sediment, whereas a steep slope tends to transport sediment across-shelf. Thus, the evolution of the subaerial delta and the growth of shoals are accelerated by a gentle slope and decelerated by a steep slope.

The effect of sediment supply on the evolution of the deltaic system was revealed by the comparison of the reference run (Figure 9a) with cases SL (Figure 9e) and SH (Figure 9f) for the low and high supplies, respectively. A significant influence was found on the extents of the subaerial delta and subaqueous delta. An extremely wide deltaic system evolved in case SH,

whereas the width greatly decreased in case SL, although the northern and southern extensions of the deltaic system were similar in those cases. The front of the southern subaerial delta was composed of a series of parallel nearshore shoals in case SL, whereas they were integrated as a whole in case SH. The simulation illustrates that an abundant sediment supply was beneficial for the rapid progradation of the delta, through the acceleration of the merging of nearshore shoals with the mainland. The results show good agreement with the perspective that sediment supply can affect the progradation rates and positions of deltas (Zhang et al., 2014). In addition, the comparisons show that an abundant sediment supply also favors the growth of offshore shoals, as the number of offshore shoals increased with the increase in sediment supply.

Once the amount of sediment feeding the deltaic system was kept constant, deviations such as the c/q ratio (Figure 9d) and the temporal variation in sediment concentration (Figure 9g) did not have an obvious influence on the distribution and development of the deltaic system. The influences were limited to the evolution of the offshore shoals. Thus, the importance of the variability of water discharge and sediment concentration was relatively minor in comparison with the effect of the total sediment availability.

Figure 9. Sensitivity analysis results of the pattern of the delta under different scenarios after a 277-year simulation. Figures (a) ~ (i) represent the results of the reference run and other cases. The name of the scenario is listed. The subaerial and quasi-subaqueous portions are bounded by red lines and dotted black lines, respectively. The criteria for determining the subaerial and subaqueous portions were the 0-m isobath and the 3-m depositional thickness, respectively.

Regarding the effect of tidal hydrodynamics, distinct variations in the delta pattern can be observed (Figures 9h, i). The shape of the simulated AYD in case WL was similar to that of the

29

modern Yellow River delta (with two main branches and shaped like a bird's foot). However, the shape of the deltaic system was extremely elongated in case WH, with a large number of parallel shoals. This may be due to a different sediment-carrying capacity associated with a different strength of hydrodynamics. If the tide is strengthened, the sediment derived by the OYR is transported by the alongshore tidal current (case WH) rather than being deposited around the river mouth (case WL). In addition, the different shapes of the deltaic system indicate that the dominant hydrodynamic forces were different in those cases, thus the relative strength ratio between the tidal forcing and the fluvial forcing is responsible for the classification of the delta. Features of a fluvial-dominated delta and a tide-dominated delta are shown in cases WL and WH, respectively. Thus, the special elongate-shaped subaerial delta and the huge area of the subaqueous delta of the AYD are determined by the moderate energetic tidal regime.

Figure 10. Sensitivity analysis results of the accumulated thicknesses of sediment under different scenarios after a 277-year simulation. The name of the scenario is listed. The quasi-subaqueous portion is bounded by black lines that represent the 3-m depositional thickness.

3.2.2 Size of the deltaic system

In this section, the quantitative analyses on the feedback of produced morphologies of delta by uncertain factors (e.g., sediment discharge) are reported. Based on our study results (i.e., Figure 9), tidal strength predominantly governs the overall patterns of a fine sediment deltaic systems. On the other hand, previous studies have stated that the tidal regime near the Jiangsu coast has remained stable over thousands of years (e.g., Zhu, 1998; Wang et al., 2012), which means that the tidal forcing setting in the reference run is dependable (section 2.3.2). Therefore, only the other six scenarios are compared with the reference run to evaluate the influence.

Figure 11. (a) Sensitivity analysis results of the area of the total delta, subaerial delta and quasi-subaqueous delta after 277-year simulations of different scenarios. The abbreviations for the scenarios listed on the X-axis are similar to those in Table 3. The dashed lines denote the estimated values of the reference run. (b) Comparison of the sediment contribution on the subaerial and quasi-subaqueous deltas. The ratios of the subaerial and subaqueous deltas accounting for the total delta are shown in different colors. The dashed lines denote deviations of ±3% from the results of the reference run.

The influence of the initial bed slope variability on the overall area of the delta was not obvious (Figure 11a, see cases BL and BH), whereas it had a significant influence on the relative area ratio between the subaerial and subaqueous deltas (Figure 11b, see cases BL and BH). A relatively gentle slope is beneficial for the progradation of the subaerial delta (Figure 9b). Thus, the relative area ratio of the subaerial delta increased in case BL. Conversely, a relatively steep slope is beneficial for cross shore sediment transport (Figure 9c). Consequently, the relative area ratio of the subaerial delta decreased in case BH. The results generally agree with the view that the mode of accommodation for deposition has a considerable effect on the evolution of a delta (Orton and Reading, 1993), especially the size of the subaerial delta (Kim et al., 2009). In addition, we highlight that accommodation mode is a critical parameter for determining the relative development of the subaerial or subaqueous portions of a deltaic system, whereas its effect on the size of the subaerial delta is secondary compared to the effect of sediment availability.

The changes in the area of the delta in cases SL and SH are considerable in comparison with other considered uncertainties (Figure 11a). It indicates that sediment availability is a key factor governing the size of deltas. However, the relative area ratio of the subaerial and subaqueous

portions in the deltaic system in cases SL and SH was similar to that in the reference run, with a deviation less than 3% (Figure 11b). Thus, we suggest that the status of the relative ratio between the subaerial and subaqueous portions is mainly governed by the marine hydrodynamic conditions and the duration of hydrodynamic action. The influence of the c/q ratio (case WS) on the delta size (on both the total absolute area and the relative ratio between the subaerial and subaqueous deltas) can be ignored, according to our results (Figure 11). In addition, the temporal variation in sediment concentration (Figure 11, see case VV) was also seen to have minimal effect on the size of the deltaic system.

In conclusion, the bed slope of the initial bathymetry influenced the possible sedimentation areas, and eventually determined the relative distributions and sizes of the subaerial and the subaqueous deltas. The availability of sediment supplied to the delta played a key role in determining the progradation rate and the size of the whole deltaic system, whereas it contributed little to the ratio of the subaerial and subaqueous areas. Once the overall amount of sediment supply was constant, variations such as the c/q ratio and the temporal variation in sediment concentration had little influence on the final evolution of AYD. Local marine hydrodynamics play a remarkable role in determining the shape and classification of a deltaic system.

4. Discussion

4.1 Reliability of the reference run

Chen et al. (2015) suggested that an exploratory model cannot be fully verified. However, historical records and maps can offer references to explore the degree to which simulations match historical evolution. In this study, the simulated 0-m isobath was defined as the shoreline. The

simulated shoreline for 1855 AD was quantitatively compared with the reference shorelines collected from the literature (e.g., Zhang, 1984; Gao, 2009). The comparison is shown in Figure 12. Despite a series of uncertainties and simplifications of the model parameters, the general shape of the shoreline simulated by the reference run was comparable to the historical data.

Despite the good agreement between the overall shorelines, the protruding pattern of the shoreline for 1855 AD near the river mouth was not well reproduced by the reference run (Figure 12). However, the simulated protuberance had quite good agreement with the shoreline in the 1890s. We suggest that there are mainly two reasons that led to the deviation between the simulations and the reference shoreline of 1855 AD. On the one hand, it may have been due to the schematizations of the model for uncertainty, e.g., neglecting the wave influence and local detailed geological features around the river mouth. On the other hand, the reference shoreline of 1855 AD may not have been as accurate as expected. The historical maps shown in Figure 13 were painted following a traditional Chinese cartography method (Ji li hua fang)[1], and are suggested to be more reliable than the maps shown in the Appendix. It is noteworthy that both historical maps clearly show the curvilinear shoreline near Yangkou (Figure 13). However, no protruding feature near the river mouth can be seen in the two historical maps. Therefore, we suggest that the modeled result with a moderate protuberance around the river mouth might be more reliable.

A highlighted feature in the historical drawings is the dense channel network (Figure 13 and Appendix). In comparison with the historical maps, the subaerial delta (bed elevation > 0 m) was also simulated as a complicated system composed of merged shoals and tidal channels (Figure

---

[1]Ji li hua fang: use a series of squares as grids, ignoring the curvature of the earth surface. The scale of the map is according to the length of the square. For example, the scale of figure 13b is that each square denotes 50 km×50 km.

12). Thus, this feature was well reproduced by the model. Note that the simulated delta more south of 33.3°N lacked this feature, primarily as a result of the grid resolution, which was relatively high near the river mouth and low in the farther regions.

Another feature shown on the historical maps is the existence of a number of shoals. On the "Qing Empire's complete map of all under heaven" historical map (Figure 13b), a series of shoals is highlighted along the Jiangsu Coast, from 33°N to 34°N. In our model, the same region outside the mainland was comprised of both the subaerial and subaqueous portions (Figure 6f). Thus, this morphological feature exhibited in the historical maps was also well captured, regardless of whether the shoals on the historical map are subaerial or subaqueous shoals. With respect to the pictorial historical maps (see Appendix), although the shape of shoals was drawn differently, the three regions with shoals can be summarized as being (1) northeast of the OYR's river mouth, (2) in the central part of the Jiangsu Coast and (3) in the southernmost region of the Jiangsu Coast. The model simulations generally reproduced the distribution of the shoals (Figure 6f), with the exception of the southernmost region. These poorly modeled shoals may have been due to an inappropriate setting of the sediment input through the southern open boundary, which in reality may have been discharged by the Yangtze River. In addition, the southernmost shoals were near the boundary of our model, which is out of the scope of our interest.

In conclusion, the simulated AYD in the reference run was comparable with the historical maps, despite the uncertainties and schematization in the model. Therefore, the evolutionary process and dynamic mechanism of the delta simulated by the reference run are expected to be reliable.

Figure 12. Simulated shoreline for 1855 AD in comparison with the reference shorelines. In this study, the shoreline was delineated by the 0-m isobath (orange lines). The blue and black lines are the reference shorelines for 1855 AD (modified after Zhou et al., 2014) and for the 1890s (modified after Zhang, 1984; Gao, 2009), respectively.

Figure 13. (a) Part of the "Huang yu quan tu" historical map, which was drawn between 1721 and1722 AD. It is the first Chinese national map painted with longitudinal and latitudinal grids and has a scale of 1:400,000. The digital version is available at *http://www.loc.gov/item/2002626779/*. (b) Part of the "Qing Empire's complete map of all under heaven" historical map, which was drawn between 1832 and 1842 AD. The digital version is available at: *http://www.loc.gov/item/gm71005054/*. The shoals drawn on the map were highlighted. Important geographic positions are indicated by the OYR, Yangkou and the Yangtze River to distinguish the boundary of the Jiangsu Coast.

It is suggested that a process-based morphological model is valuable if the model parameters are in a reasonable range (Van der Wegen et al., 2011). To assess the reasonability of the uncertainty, the results of the scenarios were compared with the historical maps and the results of the existing geological surveys. Because the simulated shoreline of the reference run was verified to agree well with the historical maps (Figure 12), the large variation in the simulated subaerial delta for case SL and case SH was not realistic. Consequently, the amount of sediment supply in the reference run is considered to be more reasonable. Furthermore, the detailed OYR-derived sediment and water discharge are hard to be determined, because the influence of the c/q ratio and the temporal variation in sediment concentration on the morphological evolution of the AYD are small. Nevertheless, we suggest that it is possible to use a representative sediment concentration, similar to the representative tide, to reduce the computational effort of a long-term morphological model to a reasonable level. In addition, a moderate modification of the c/q ratio in view of the lack of data is acceptable for generating reliable long-term morphology changes. On the other hand, we have demonstrated that the amount of sediment supply has little influence

on the relative ratio of the area between the subaerial and subaqueous deltas in a deltaic system. Thus, the area of the subaqueous delta simulated by the reference run is considered as reliable, based on the reliable simulation of the subaerial delta, when other uncertain factors do not change. Regarding the geological position of the subaqueous delta, the results of the reference run, rather than cases BL and BH (i.e., the effect of the initial bed slope), are in agreement with the geological surveys (Figure 3b). Therefore, the setting of the slope of the initial bathymetry in the reference run is also suggested to be appropriate. In summary, we suggest that the reference run settings are representative for reproducing the historical maps.

Furthermore, our present model is a schematized model. The requirement for a quantitatively accurate value for each parameter in a schematized (or idealized) model is not as high as for a realistic model. A recent study of van Maren et al. (2016) discussed the influence of equifinality on predictive model capabilities. Equifinality denotes different combinations of model input parameters that lead to the same result. Note that these various model parameter sets can affect the transport processes. The results demonstrate that the influence of equifinality model settings is quite weak, which strengthens confidence in the numerical model predictions. Regarding our study, we emphasize that the set of parameters, rather than each parameter adopted in the reference run, is reasonable.

4.2 Suggestion on the spatial distribution of the AYD

As mentioned in section 2.2, there are many controversial perspectives on the delta distribution, indicating limited hindcast understanding of the AYD. According to the reference run, the area of subaerial delta, formed from 1578 to 1855 AD, is simulated as 0.90×10^4 km^2. The area formed from 1128 to 1578 AD is calculated as 0.74×10^4 km^2, based on the reference shoreline of 1127

AD and 1578 AD (Gao, 2009). Thus, the total subaerial delta of the AYD until 1855 AD is estimated to be 1.64×10^4 km^2. The area of subaqueous delta formed from 1578 to 1855 AD in the model is 0.65×10^4 km^2. Thus, we suggest the total area of the AYD should be approximately 2.29×10^4 km^2. The results have a good agreement with the estimations by Hu, Saito and Kempe (1998), which announced that the OYR formed an area of 2.70×10^4 km^2 during the 700 year period.

Figure 14. Simulated subaerial delta (bed elevation > 0 m, bounded by orange lines) and contour lines of the 3-m accumulated deposition (bounded by black lines). Several previous estimates of the scope of subaqueous delta are collected and shown with color dotted lines. The numbers of the estimates are consistent with Table 2. The two contour lines representing the 25-m and 30-m isobaths (according to the simulated results for 1855 AD) are shown as dashed dark green lines. Several important geographic sites are noted, including the Guanhe estuary, Xinyang Gang and Yangkou, according to their present locations.

The simulated distribution of the subaerial delta is shown in Figure 14. The northern boundary of the subaerial delta extends to approximately 34°33′N, near the Guanhe estuary. The southern boundary reaches the present location of the radial sand ridge field near Yangkou. According to the locations of the southern and northern boundaries, the simulated results are in a reasonable agreement with viewpoint V in Table 1 and Figure 3a. Furthermore, the seaward extension of the subaerial delta was simulated to be 43 km from 1578 to 1855 AD. Because data on the seaward extension of the river mouth are scarce, geological field investigations are suggested in future research to validate the simulation.

The distribution of the quasi-subaqueous delta, shown in Figure 14, is wide in the north and thin in the south, similar to the shape for the viewpoint ⑨ in Table 2 and Figure 4. However, after

comparison with the boundary of the subaerial delta, the "thin" southern quasi-subaqueous delta is more like submerged shoals or the face of the subaerial delta. Thus, we consider that the subaqueous delta was distributed between 33.7°N and 34.8°N. In general, although the distribution asymmetry of the subaerial delta is significant, the distribution of the subaqueous delta is shown as completely symmetrical. The simulated northern boundary agreed well with most of the previous viewpoints (Table 2). The simulated southern boundary was near the Xinyang Gang (see the location in Figure 14), which is in accordance with estimate ⑦ (Table 2). Furthermore, the seaward boundary of the subaqueous delta was simulated to be located between the 25-m and 30-m isobaths (according to the simulated results for 1855 AD) and was approximately 86~110 km in width (Figure 14). Assuming the seaward extension between 1128 and 1578 AD did not exceed the extension between 1578 and 1855 AD, the total progradation distance was in reasonable agreement with estimates ⑦ and ⑫ (Table 2). Thus, geologically based viewpoint ⑦ in Table 2 is generally indicated to be in satisfactory agreement with the simulations for the subaqueous delta of the AYD. It should be highlighted that in addition to evaluating and validating the previous geological estimations, our results provide better-detailed geometric features for the distribution of the AYD.

4.3 Limitation of this study

The model ignored waves and short term events (e.g., storms and floods). The wave climate, which consists mostly of locally wind-generated waves (Huang et al., 2005), may have some impact on the evolution of the shallow water regions and shaping the shoreline (Geleynse et al., 2011). Xing et al. (2012) and Zhang et al. (1999) have conducted many investigations on the effects of tides, waves, winds, etc. on the sediment transport and morphological evolution of the Jiangsu Coast. According to the results of Xing et al. (2012), the suspended sediment

concentration (SSC) is much lower (the deviation is approximately 100%) in the absence of tides, whereas the average deviation of the SSC is only 6% and 5%, when winds and waves, respectively, are ignored (taking the SR4 station in Xing et al. (2012) as an example, which is the nearest station to the AYD). The maximum deviations of the SSC contributed by relatively stronger winds and waves are still less than 13% and 9%, respectively. Xing et al. (2012) addressed that, for the whole Jiangsu coast, tide is the dominant factor that determines the SSC, whereas winds and waves only influence minor fluctuations of the SSC. Similarly, Zhang et al. (1999) stated that waves only influence local-scale rather than gross-scale morphologies, and that the effects of waves are secondary in comparison with the effects of tides.

Figure 15 shows an examination of the hydrodynamic conditions for relevant coastal environments. The criterion was adopted from the classification of delta proposed by Orton and Reading (1993), which takes the effects of grain size into account. Note that the vertical and horizontal axes of the criterion are the mean tidal range and mean wave height, respectively. The present mean wave height near the abandoned Yellow River mouth was estimated to be 0.52 m by Qiu (2006) and 0.6 m by Xu and Yu (1999). The mean tidal range of the Jiangsu coast is approximately 2~6 m (Wang and Ke, 1997). Thus, the zone representing the AYD (in the recent period) is located above the criterion curve (Figure 15). Consequently, the AYD at present is demonstrated to be a tidal-dominated delta. According to our model, the amplitude of the M2 tide was approximately 0.8 m in the vicinity of the river mouth in 1578 (Figure 5). Considering the other tidal components, the tidal range is expected to also exceed 2 m for the deltaic system. Given that changes in wave conditions have not been obvious in the past hundreds of years, the AYD can also be classified to have been a tidally dominated system during the progradation stage. A change in the classification of the delta (i.e., changing from a tidally dominated delta to a

mixed energy delta) requires that the mean wave height exceeded 1.65 m (Figure 15). However, the frequency for $H_{1/10}$ larger than 1.5 m near the AYD is only 11.59% (Xu, 2005). It is expected that the possibility for a mean wave height larger than 1.65 m is extremely small. Even for a period coinciding with the Little Ice Age from 1578 to 1855, we suggest that it is still highly improbable that the mean wave height during the historical period could have been more than three times larger than that at present (i.e., more than 1.5 m). Moreover, Galloway (1975) emphasized that deltaic progradation is modified primarily by tidal currents and wave surge, although oceanic and wind-generated currents and storm surges also occur in marine environments. Therefore, among various hydrodynamic forces, tides were most important for the progradation of the AYD.

From a geological perspective, a cuspate feature of a subaerial delta is usually formed where a river debouches on a straight coastline and in which the sedimentary material is deposited evenly on either side of the river mouth owing to strong waves (Bharatdwaj, 2009). Cuspate deltas are also called wave-dominated deltas. Many lines of evidence from the previous literature have shown that the suspended sediment of the AYD is mainly transported southeastward (Alexander et al., 1991, Milliman et al., 1985, Milliman et al., 1987, Hu et al., 2011, Kim et al., 2013, Zhou et al., 2014). The disposition feature of the AYD does not match that of a cuspate delta, viz. the AYD is not a wave-dominated delta. On the other hand, subaqueous clinoforms are formed in shallow marine environments, and basin hydrodynamics (e.g., waves, tides and currents) are all responsible for driving sediment advection (Pirmez et al., 1998, Driscoll and Karner, 1999, Adams and Schlager, 2000, Hernández-Molina et al., 2000, Cattaneo et al., 2003, Swenson et al., 2005, Mitchell et al., 2012). Liu et al. (2013) emphasized that lower hydrodynamic energy is not favorable for such clinoforms to develop. Therefore, focusing on the energetic hydrodynamic

factor(s) with respect to the development of a clinoform is reasonable. As we previously mentioned, the AYD in its progradation stage is classified as a tidally dominated delta. Both Zhang et al. (1999) and Su et al. (2016) demonstrated that the effect of waves on the gross-scale morphological changes of the Jiangsu coast is secondary and only reflected by local-scale morphological changes. Therefore, in this study, we simplified the model by only considering tides. Nevertheless, although we have demonstrated that tides are the predominant factor, it is worthwhile to explore the influence of waves, storms and floods on the shape and evolution of AYD in the future.

The influence of the simplifications of other parameters such as sea level rise and the sediment properties of the OYR on the evolution of the AYD has not been assessed in this study. Although the sediment cohesiveness has been suggested as an important factor for delta evolution (Edmonds and Slingerland, 2009), we assumed that it did not change much during the past centuries (coming from Loess Plateau) and that any possible changes could not have been sufficiently significant to have influenced the delta progradation of the AYD. These limitations could be remedied in the future.

Figure 15. General relationships between wave height and tidal range for clay-silt sediments for determining the tide-dominated delta (Modified after Davis and Hayes, 1984; Orton and Reading, 1993). The dots for the AYD is based on the simulated M2 tide amplitude in this study and the measured multi-year averaged wave parameters in Lianyungang during 1961 and 1968 (Qiu, 2005). The data for the Modern Yellow River delta, Yangtze River delta and the Amazon River delta refers to Coleman and Wright (1975), Wang and ke (1989), Yan et al. (1989), and Milliman and Meade (1983).

5. Conclusions

The evolution of a deltaic system is sensitive to modifications in environmental parameters such as fluvial discharge, mode of accommodation and sediment supply. The AYD, which was formed by the OYR from 1128 to 1855 AD, is now undergoing a severe erosion process because of the abrupt cessation of the sediment supply. Geological approaches are insufficient to provide a comprehensive understanding of the progradation process of the AYD, including the distribution of the deltaic system and the deposition of sediment derived by the OYR. To investigate the morphodynamic evolution of such a fine grain size delta and to provide reliable fundamental data for analyzing the subsequent erosional processes, a process-based morphological model was applied to reproduce a reliable progradation of the AYD. Owing to the scarcity of historical data, several alternative sources such as historical records, maps and geological survey estimations were combined in this study.

The simulation results show that the progradation mechanism of the AYD has varied spatially and temporally. For the northern and southern parts of the delta, the progradation modes were different. The progradation of the southern delta was by means of the growth of shoals and subsequent merging with the mainland, whereas the shoals in the northern part gradually became isolated and were independent of the progradation of the northern delta. Based on the analysis of the residual sediment transport, the emphasis on the progradation of the deltaic system changes from the rapid expansion of the southern delta to the development of shoals in the northern part during the period of a 100-year to 200-year simulation. The distribution of the subaerial delta and the deposition of the sediment derived by the OYR show a significant asymmetrical feature. However, the subaqueous delta is suggested to have a relatively symmetric distribution pattern.

Uncertainties in model settings are inevitable because of the lack of historical data. Scenarios were designed and carried out to investigate the influence of uncertainties on the development and distribution of the delta, including the effect on the contributions of the subaerial and subaqueous deltas. The tidal regime is suggested to be the key factor that determines the type and principle evolutionary trend of the delta. Sediment supply dominates progradation rate and the size of delta, whereas the relative area ratio between the subaerial and subaqueous deltas is independent of sediment availability. In contrast, the accommodation slope has a considerable effect on determining the distribution location of the deltaic system and the relative ratio between the subaerial and the subaqueous deltas, whereas its effect on the overall area of the delta is secondary compared to sediment availability. The effects of the c/q ratio and the temporal variation in sediment concentration have been demonstrated to be minor for the evolution of the deltaic system.

Detailed comparisons between the simulation results and the historical data revealed that the reference run in the present study can reconstruct the AYD with a satisfactory reliability. The analysis of the effects of uncertainties on the morphological evolution of the delta suggests that the settings of the uncertain parameters in the reference run were acceptable. Subsequently, suggestions on the size of the AYD (until 1855 AD) were provided.

In contrast with geological findings, the simulation results provide comprehensive fundamental information (e.g., reliable bathymetry data) for analyzing the subsequent severe erosion of the AYD since 1855 AD. Future work, apart from assessing the sensitivity of the results to the unconsidered uncertain factors, will focus on the erosion stage of the AYD and on the contribution of the AYD's erosion to the evolution of the radial sand ridges.

Acknowledgements

Reference

Atlas of the Oceans Editorial Board, 1993. Marine Atlas of the Bohai Sea, Yellow Sea and East China Sea (Hydrological). The Ocean Press, Beijing (in Chinese).

Anthony, E. J., 2015. Wave influence in the construction, shaping and destruction of river deltas: A review. Mar. Geol., 361, 53-78.

Batalla, R. J., Vericat, D., Tena, A., 2014. The fluvial geomorphology of the lower Ebro (2002-2013): Bridging gaps between management and research. Cuadernos de investigación geográfica, (40), 29-51.

Caldwell, R., Edmonds, D., 2014. The effects of sediment properties on deltaic processes and morphologies: A numerical modeling study. J. Geophys. Res. Surf. 119, 961–982. doi:10.1002/2013JF002965.

Cayocca, F., 2001. Long-term morphological modeling of a tidal inlet: the Arcachon Basin, France. Coast. Eng., 42(2), 115-142.

Chen, K.F., Wang, Y.H., Lu, P.D., Zheng, J.H., 2009. Effects of coastline changes on tide system of Yellow Sea off Jiangsu coast, China. China Ocean Eng. 23, 741–750.

Chen, X.X., Miao, J.Y., Song, Y.Q., 1993. A preliminary study of Huaihe River delta. Mar. Sci. 4, 10–13 (in Chinese with English abstract).

Chen, Y., Overeem, I., Kettner, A.J., Gao, S., Syvitski, J.P.M., 2015. Modeling Flood Dynamics along the Super-elevated Channel Belt of the Yellow River over the Last 3000 years. J. Geophys. Res. Earth Surf. doi:10.1002/2015JF003556 (accepted)

Cheng, G.D., Xue, C.T., 1997. Sedimentary Geology of the Yellow River Delta. Geological Publishing House, Beijing (in Chinese).

Chinese Ministry of Water Resources, 2011. Chinese river sediment bulletin. Beijing (in Chinese).

Coco, G., Zhou, Z., van Maanen, B., Olabarrieta, M., Tinoco, R., Townend, I., 2013. Morphodynamics of tidal networks: advances and challenges. Mar. Geol. 346, 1-16.

Coleman, J. M., Roberts, H. H., Stone, G. W. 1998. Mississippi River delta: an overview. J Coastal Res, 699-716.

Coleman, J.M., Wright, L.D., 1975. Modern river deltas: variability of processes and sand bodies. In: Deltas: Models for Exploration (Ed. by M. L. Broussard), pp. 99-149. Houston Geological Society.

Dastgheib, A., Roelvink, J. A., Wang, Z.B., 2008. Long-term process-based morphological modeling of the Marsdiep Tidal Basin. Mar. Geol. 256, 90–100.

Davis, R.A., Hayes, M.O., 1984. What is a wave-dominated coast? Mar. Geol. 60, 313–329.

Deltares, 2012. Delft3D-FLOW user manual.

De Vriend, H., Capobianco, M., Chesher, T., de Swart, H.E., Latteux, B., Stive, M.J.F., 1993. Approaches to long-term modelling of coastal morphology: a review. Coast. Eng. 21, 225–269.

Dissanayake, D.M.P.K.,Roelvink, J.A., 2007. Process-based approachontidal inlet evolution—part 1. Proceedings RCEM conference, Vol.1. Enschede, The Netherlands, pp. 3–9.

Dissanayake, D.M.P.K., Roelvink, J. A., van der Wegen, M., 2009. Modelled channel patterns in a schematized tidal inlet. Coast. Eng. 56, 1069–1083. doi:10.1016/j.coastaleng.2009.08.008

Edmonds, D. A., Slingerland, R.L., 2009. Significant effect of sediment cohesion on delta morphology. Nat. Geosci. 3, 105–109. doi:10.1038/ngeo730

Edmonds, D., Slingerland, R., Best, J., Parsons, D., Smith, N., 2010. Response of river‐dominated delta channel networks to permanent changes in river discharge. Geophys Res Lett 37(12).

Frihy, O.E., Shereet, S.M., El Banna, M.M., 2008. Pattern of Beach Erosion and Scour Depth along the Rosetta Promontory and their Effect on the Existing Protection Works, Nile Delta, Egypt. J. Coast. Res. 24, 857–866. doi:10.2112/07-0855.1

Gao, S., 2009. Modeling the preservation potential of tidal flat sedimentary records, Jiangsu coast, eastern China. Cont. Shelf Res. 29, 1927–1936.

Gao, S.M., Li, Y.F., An, F.T., 1989. The Formation and Sedimentary Environments of theYellow River Delta. Science Press, Beijing (in Chinese).

Geleynse, N., Storms, J.E. A., Stive, M.J.F., Jagers, H.R. A., Walstra, D.J.R., 2010. Modeling of a mixed-load fluvio-deltaic system. Geophys. Res. Lett. 37. doi:10.1029/2009GL042000

Geleynse, N., Storms, J.E. A., Walstra, D.J.R., Jagers, H.R.A., Wang, Z.B., Stive, M.J.F., 2011. Controls on river delta formation; insights from numerical modelling. Earth Planet. Sci. Lett. 302, 217–226. doi:10.1016/j.epsl.2010.12.013

Gelfenbaum, G., Stevens, A., Elias, E., Warrick, J., 2009. Modeling Sediment Transport and Delta Morphology on the Dammed Elwha River, in: 6th Proceedings of Coastal Dynamics. pp. 1–15.

Giosan, L., 2007. Morphodynamic feedbacks on deltaic coasts: Lessons from the wave-dominated Danube delta, in: Proceedings of Coastal Sediments. pp. 1–14.

Guo, L.C., 2014. Modeling estuarine morphodynamics under combined river and tidal forcing. TU Delft, Delft University of Technology.

Guo, L.C, van der Wegen, M., Roelvink, J.A., He, Q., 2015. Exploration of impacts of seasonal river discharge variations on long-term estuarine morphodynamic behavior. Coastal Engineering 95, 105–116.

Hanebuth, T.J.J., Proske, U., Saito, Y., Nguyen, V.L., Ta, T.K.O., 2012. Early growth stage of a large delta — Transformation from estuarine-platform to deltaic-progradational conditions (the northeastern Mekong River Delta, Vietnam). Sediment. Geol. 261-262, 108–119. doi:10.1016/j.sedgeo.2012.03.014

Hu, C.H., Cao, W.H., 2003. Variation, regulation and control of flow and sediment in the Yellow River Estuary: I. Mechanism of flow-sediment transport and evolution. J. Sediment Res. 5, 1–8 (in Chinese with English abstract).

Hu, D., Saito,Y. and Kempe, S., 1998. Sediment and nutrient transport to the coastal zone. Asian change in the context of global climate change: impact of natural and anthropogenic changes in Asia on global biogeochemical cycles 3, 245-270.

Huang, H.J., Li, F., Pang, J.Z., 2005. Study on the Land-Ocean Interaction between the Yellow River Delta and the Bohai and the Yellow Seas. Science Press, Beijing (in Chinese).

Jiménez, J. A., Sánchez-Arcilla, A., Valdemoro, H., 1997. Processes reshaping the Ebro delta. Mar. Geol. 144, 59–79.

Jiménez, J. A., Sánchez-Arcilla, A., 2004. A long-term (decadal scale) evolution model for microtidal barrier systems. Coast. Eng. 51(8), 749-764.

Karunarathna, H., Reeve, D., Spivack, M., 2008. Long-term morphodynamic evolution of estuaries: an inverse problem. Estuar Coast Shelf S 77, 385–395.

Kim, W., Dai, A., Muto, T., Parker, G., 2009. Delta progradation driven by an advancing sediment source: Coupled theory and experiment describing the evolution of elongated deltas. Water Resour. Res. 45, w06428. doi:10.1029/2008WR007382

Kleinhans, M.G., Weerts, H.J.T., Cohen, K.M., 2010. Avulsion in action: Reconstruction and modelling sedimentation pace and upstream flood water levels following a Medieval tidal-river diversion catastrophe (Biesbosch, The Netherlands, 1421–1750AD). Geomorphology 118, 65–79. doi:10.1016/j.geomorph.2009.12.009

Lesser, G.R., Roelvink, J. A., van Kester, J. A. T.M., Stelling, G.S., 2004. Development and validation of a three-dimensional morphological model. Coast. Eng. 51, 883–915. doi:10.1016/j.coastaleng.2004.07.014

Li, C.X., Zhang, J.Q., Fan, D.D., Deng, B., 2001. Holocene regression and the tidal radial sand ridge system formation in the Jiangsu coastal zone, East China. Mar. Geol. 173, 97–120.

Li, F., Li, Y.Z., Zhang, X.R., 2001. Impact of variation of water and sediment fluxes on sustainable use of marine environment and resources in the Huanghe river estuary and adjacent sea Ⅲ. Imapct of long-term stabilization of the lower course of the Huanghe river on the construction of coas. Stud. Mar. Sin. 42, 68–82 (in Chinese with English abstract).

Li, W., van Maren, D.S., Wang, Z.B., de Vriend, H.J., Wu, B.S., 2014. Peak discharge increase in hyperconcentrated floods. Adv. Water Resour. 67. 65-77.

Li, Y.F., 1991. The development of the abandoned Yellow River Delta. Geogr. Res. 10, 29–39 (in Chinese with English abstract).

Lim, D.I., Choi, J.Y., Jung, H.S., Rho, K.C., Ahn, K.S., 2007. Recent sediment accumulation and origin of shelf mud deposits in the Yellow and East China Seas. Prog. Oceanogr. 73, 145–159. doi:10.1016/j.pocean.2007.02.004

Liu, J., Kong, X., Saito, Y., Liu, J.P., Yang, Z., Wen, C., 2013. Subaqueous deltaic formation of the Old Yellow River (AD 1128–1855) on the western South Yellow Sea. Mar. Geol. 344, 19–33. doi:10.1016/j.margeo.2013.07.003

Liu, J., Saito, Y., Kong, X., Wang, H., Xiang, L., Wen, C., Nakashima, R., 2010. Sedimentary record of environmental evolution off the Yangtze River estuary, East China Sea, during the last ∼13,000 years, with special reference to the influence of the Yellow River on the Yangtze River delta during the last 600 years. Quat. Sci. Rev. 29, 2424–2438. doi:10.1016/j.quascirev.2010.06.016

Liu, T., Shi, X., Li, C., Yang, G., 2012. The reverse sediment transport trend between abandoned Huanghe River (Yellow River) Delta and radial sand ridges along Jiangsu coastline of

China—an evidence from grain size analysis. Acta Oceanol. Sin. 31, 83–91. doi:10.1007/s13131-012-0255-3

Liu, X., 2011. The coastal erosion of the abandoned Yellow River Delta in northern Jiangsu province, China: Based on analysis of remote sensing images, in: 19th International Conference on Geoinformatics. pp. 1–5.

Luijendijk, A.P., Bos, K.J., Venuti, A., Serafini, E., Passacantando, D., Brotto, M.T., 2004. Numerical and physical modelling of scour development at the Malamocco inlet, in: Proceedings of 2nd International Conference on Scour and Erosion. Singapore, pp. 1–8.

Maa, J.P., Kwon, J., Hwang, K., Ha, H., 2008. Critical Bed-Shear Stress for Cohesive Sediment Deposition. J. Hydraul. Eng. 134, 1767–1771.

Milliman, J.D., Yun-Shan, Q., Mei-e, R., Saito, Y., 1987. Man's influence on the erosion and transport of sediment by Asian rivers: the Yellow River (Huanghe) example. J. Geol. 95, 751–762.

Milliman, J.D., Farnsworth, K.L., Jones, P.D., Xu, K. H., Smith, L.C., 2008,Climatic and anthropogenic factors affecting river discharge to the global ocean, 1951–2000, Global Planet. Change, 62(3–4), 187–194, doi:10.1016/j.gloplacha.2008.03.001.

Milliman, J.D., Meade, R.H., 1983. World wide delivery of sediment to the oceans. J. Geol., 91, 1-21.

Nguyen, D., Etri, T., Runte, K.H., Mayerle, R., 2010. Morphodynamic modeling of the medium-term migration of a tidal channel using process-based model, in: Proceedings of 32nd Conference on Coastal Engineering. Shanghai, pp. 1–13.

Nienhuis, J.H., Ashton, A.D., Roos, P.C., Hulscher, S.J.M.H., Giosan, L., 2013.Wave reworking of abandoned deltas. Geophys. Res. Lett. 40, 5899–5903.

Orton, G., Reading, H., 1993. Variability of deltaic processes in terms of sediment supply, with particular emphasis on grain size. Sedimentology 40, 475–512.

Park, S., Lee, H., Han, H., Lee, G., Kim, D., Yoo, D., 2000. Evolution of late Quaternary mud deposits and recent sediment budget in the southeastern Yellow Sea. Mar. Geol. 170, 271–288.

Partheniades, E., 1965. Erosion and Deposition of Cohesive Soils. J. Hydraul. Div. 91, 105–139.

Qiu, J.F., 2005. The study of wave and wind fields of Jiangsu Coastline. Msc thesis. Hohai University (in Chinese with English abstract).

Ranasinghe, R., Swinkels, C., Luijendijk, A., Roelvink, D., Bosboom, J., Stive, M., Walstra, D., 2011. Morphodynamic upscaling with the MORFAC approach: Dependencies and sensitivities. Coast. Eng. 58, 806–811. doi:10.1016/j.coastaleng.2011.03.010

Ren, M.E., Shi, Y., 1986. Sediment discharge of the Yellow River (China) and its effect on the sedimentation of the Bohai and the Yellow Sea. Cont. Shelf Res. 6, 785–810.

Ren, M.E., 1987. Modern sedimentation in the coastal and nearshore zones of China. Springer Verlag.

Ren, M.E., 2006. Sediment discharge of the Yellow River, China: past, present and future-A Synthesis. Adv. earth Sci. 21, 551–563 (in Chinese with English abstract).

Ren, M.E., Zeng, Z.X., Cui, G.H., 1994. China's Three Biggest Deltas. Higher Education Press, Beijing.

Roberts, H.H., 1997. Dynamic changes of the Holocene Mississippi River delta plain: the delta cycle. J. Coastal Res. 13, 605–627.

Roelvink, J.A., 2006. Coastal morphodynamic evolution techniques. Coast. Eng. 53, 277–287. doi:10.1016/j.coastaleng.2005.10.015

Roelvink, J.A., Reniers, A.J.H.M., 2011. A guide to coastal morphology modeling. Advances in Coastal and Ocean Engineering, vol.12, World Scientific Publishing Company, Singapore, 292 pp.

Ruggiero, P., Walstra, D.J.R., Gelfenbaum, G., van Ormondt, M., 2009. Seasonal-scale nearshore morphological evolution: Field observations and numerical modeling. Coast. Eng. 56, 1153–1172. doi:10.1016/j.coastaleng.2009.08.003

Sabatier, F., Samat, O., Ullmann, A., Suanez, S., 2009. Connecting large-scale coastal behaviour with coastal management of the Rhône delta. Geomorphology 107, 79–89.

Saito, Y., Wei, H., Zhou, Y., Nishimura, A., 2000. Delta progradation and chenier formation in the Huanghe (Yellow River) delta, China. J. Asian Earth 18, 489–497.

Saito, Y., Yang, Z.S., 1995. Historical change of the Huanghe (Yellow River) and its impact on the sediment budget of the East China Sea, in: Proceedings of International Symposium on Global Flues of Carbon and Its Realted Substances in the Coastal Sea-Ocean-Atmosphere System. pp. 7–12.

Seybold, H.J., Molnar, P., Singer, H.M., Andrade, J.S., Herrmann, H.J., Kinzelbach, W., 2009. Simulation of birdfoot delta formation with application to the Mississippi Delta. J. Geophys. Res. 114, F03012. doi:10.1029/2009JF001248

Simeoni, U., Fontolan, G., Tessari, U., Corbau, C., 2007. Domains of spit evolution in the Goro area, Po Delta, Italy. Geomorphology, 86(3), 332-348.

Shi, X.F., Liu, Y.G., Chen, Z.H., Wei, J.W., Ge, S.L., 2012. Origin, transport processes and distribution pattern of modern sediments in the Yellow Sea, in: Li, M.Z., Sherwood, C.R., Hill, P.R. (Eds.), Sediments, Morphology and Sedimentary Processes on Continental Shelves: Advances in Technologies, Research, and Applications. John Wiley & Sons Ltd, Chichester, West Sussex, UK, pp. 321–350.

Smith, B., Bjorstad, P., Gropp, W., 2004. Domain Decomposition: Parallel Multilevel Methods for Elliptic Partial Differential Equations. Cambridge University Press.

State Oceanic Administration, 2003. Chinese sea level rise bulletin, 2003. Beijing (in Chinese).

Stefani, M., Vincenzi, S., 2005. The interplay of eustasy, climate and human activity in the late Quaternary depositional evolution and sedimentary architecture of the Po Delta system. Mar. Geol. 222–223, 19–48.

Stive, M.J.F., Wang, Z.B., 2003. Morphodynamic modeling of tidal basins and coastal inlets. In: V.C. Lakham (ed.), Advances in Coastal Modelling, Elsevier Science, pp.367–392.

Su, M., Yao, P., Wang, Z.B., Zhang, C.K., Stive, M.J.F., 2015. Tidal wave propagation in the Yellow Sea. Coast. Eng. J. 57, 1550008. doi:10.1142/S0578563415500084

Swenson, J.B., 2005. Fluvial and marine controls on combined subaerial and subaqueous delta progradation: Morphodynamic modeling of compound-clinoform development. J. Geophys. Res. 110, F02013. doi:10.1029/2004JF000265

Syvitski, J.P.M., Saito, Y., 2007. Morphodynamics of deltas under the influence of humans. Glob. Planet. Change 57, 261–282. doi:10.1016/j.gloplacha.2006.12.001

Teague, W.J., Perkins, H.T., Hallock, Z.R., Jacobs, G.A., 1998. Current and tide observations in the southern Yellow Sea. J. Geophys. Res. 103, 27,783–27,793.

Tregear, T., 1965. A geography of China. University of London Press LTD.

Uehara, K., Saito, Y., Hori, K., 2002. Paleotidal regime in the Changjiang (Yangtze) Estuary, the East China Sea, and the Yellow Sea at 6 ka and 10 ka estimated from a numerical model. Mar. Geol. 183, 179–192.

Van der Wegen, M., Jaffe, B.E., Roelvink, J. A., 2011. Process-based, morphodynamic hindcast of decadal deposition patterns in San Pablo Bay, California, 1856–1887. J. Geophys. Res. 116, F02008. doi:10.1029/2009JF001614

van Maren, D. S., Cronin, K., 2016. Uncertainty in complex three-dimensional sediment transport models: equifinality in a model application of the Ems Estuary, the Netherlands. Ocean Dynam., 1-15.

Van Maren, D.S., Winterwerp, J.C., Wang, Z.Y., Pu, Q., 2009. Suspended sediment dynamics and morphodynamics in the Yellow River, China. Sedimentology 56, 785–806. doi:10.1111/j.1365-3091.2008.00997.x

Van Maren, D.S., Winterwerp, J.C., Wu, B.S., Zhou, J.J., 2009. Modelling hyperconcentrated flow in the Yellow River. Earth Surf. Process. Landforms 34, 596–612. doi:10.1002/esp

Van Rijn, L.C., 1993. Principles of Sediment Transport in Rivers, Estuaries and Coastal Seas, Aqua publications. Aqua publications, Amsterdam.

Wan, Y.S., 1989. Development and decline of ancient Huanghe River estuary delta in Northern Jiangsu. Oceanol. Limnol. Sin. 20, 66–74 (in Chinese with English abstract).

Wang, G., Xu, M., 1999. Analysis of peculiarities of 92.8 flood event in the lower Yellow River. Int. J. Sediment Res. 14, 205–213.

Wang, K.C., 1998. Study on the evolution of the tail reaches of the Abandoned Yellow River during the Ming-Qing dynasty and its patterns, in: Liu, H.Y. (Ed.), The Investigation of the Abandoned Yellow River Course during the Ming-Qing Dynasty. Hohai University Press, Nanjing, pp. 252–2 (in Chinese).

Wang, Y., Aubrey, D., 1987. The characteristics of the China coastline. Cont. Shelf Res. 7, 329–349.

Wang, Y., Ke, X., 1989. Cheniers on the east coastal plain of China. Mar. Geol., 90, 321-336.

Wang, X., Ke, X., 1997. Grain-size characteristics of the extant tidal flat sediments along the Jiangsu coast, China. Sediment Geol., 112(1), 105-122.Wang, Y., 1983. The mudflat system of China. Can. J. Fish. Aquatic Sci., 40, 160-171.

Wang, Y., Zhang, Y.Z., Zou, X.Q., Zhu, D.K., Piper, D., 2012. The sand ridge field of the South Yellow Sea: Origin by river–sea interaction. Mar. Geol. 291-294, 132–146.

Winterwerp, J.C., 2006. Stratification effects by fine suspended sediment at low, medium, and very high concentrations. J. Geophys. Res. 111, C05012. doi:10.1029/2005JC003019

Woodroffe, C.D., 2003. Coasts: Form, Process and Evolution. Cambridge University Press, Cambridge, 623 pp.

Woodroffe, C.D., Saito, Y., 2011. River-Dominated Coasts. In: Wolanski E and McLusky DS (eds.) Treatise on Estuarine and Coastal Science, Vol 3, pp. 117–135. Waltham: Academic Press.

Wright, L., Coleman, J., 1973. Variations in morphology of major river deltas as functions of ocean wave and river discharge regimes. Am. Assoc. Pet. Geol. Bull. 57, 370–398.

Wright, L.D., Coleman, J.M., 1974. Mississippi River Mouth Processes: Effluent Dynamics and Morphologic Development. J. Geol. 82, 751–778.

Wu, C.Y., Ren, J., Bao, Y., Lei, Y.P., Shi, H.Y., 2007. A long-term morphological modeling study on the evolution of the Pearl River Delta, and estuarine bays since 6000 yr B.P. The Geological Society of America 426, 199–214.

Xia, F., Zhang, Y.Z., Wang, R.F., Liu, J.P., Zhang, Z.K., Peng, X.Q., 2015. Review for the studies on sedimentation range of the Abandoned Yellow River subaqueous delta, North Jiangsu plain coast. Acta Geogr. Sin. 70, 29–48 (in Chinese with English abstract). doi:10.11821/dlxb201501003

Xing, F., Wang, Y.P., Wang, H.V., 2012. Tidal hydrodynamics and fine-grained sediment transport on the radial sand ridge system in the southern Yellow Sea. Mar. Geol., 291, 192-210.

Xu, M., Lu, P.D., 2005. Sediment movement and coastal evolution under the interaction between wave and current, Nanjing Normal University Press, Nanjing (in Chinese).

Xu, M., Yu, G.H., 1999. Study on siltation of excavated channel in Abandoned Yellow River Estuary in northern Jiangsu coast. Ninth National Symposium on Coastal Engineering (in Chinese).

Xue, C.T., 1993. Historical changes in the Yellow River delta, China. Mar. Geol. 113, 321–329.

Xue, C.T., Zhou, Y., Wang, G., 2003. Reviews of the Yellow River Delta Superlobes Since 700 BC. Mar. Geol. Quat. Geol. 23, 23–29 (in Chinese with English abstract).

Xue, C.T., Liu, J., Kong, X.H., 2011. Channel shifing of lower Yellow River in 1128-1855AD and its influence to the sedimentation in Bohai, Yellow and East China Seas. Mar. Geol. Quat. Geol. 31, 25–36 (in Chinese with English abstract).

Yan, Q., Xu, S., Shao, X., 1989. Holocene cheniers in the Yangtze delta, China. Mar. Geol.,90, 311-320.

Yang, S.Y., Jung, H.S., Lim, D. Il, Li, C.X., 2003. A review on the provenance discrimination of sediments in the Yellow Sea. Earth-Science Rev. 63, 93–120. doi:10.1016/S0012-8252(03)00033-3

Yang, S.Y., Li, C.X., Jung, H.S., Lee, H.J., 2002. Discrimination of geochemical compositions between the Changjiang and the Huanghe sediments and its application for the identification of sediment source in the Jiangsu coastal plain, China. Mar. Geol. 186, 229–241.

Yang, Z.G., 1985. Sedimentology and environment in South Huanghai Sea shelf since Late Pleistocene. Mar. Geol. Quat. Geol. 5, 1–19 (in Chinese with English abstract).

Ye, Q.C., 1986. On the development of the abandoned Yellow River delta in northern Jiangsu Province. Acta Geogr. Sin. 41, 112–122 (in Chinese with English abstract).

Yossef, M.F.M., Jagers, H.R., Vuren, S.V., Sieben, A., 2008. Innovative techniques in modelling large-scale river morphology, in: Proceeding of International Conference on Fluvial Hydraulics. Cesme, Izmir, Turkey, pp. 1065–1074.

Yu, Z.Y., Chen, D.C., Jin, L., 1986. The formation and erosion-reworking of the Abandoned Yellow River subaqueous delta, North Jiangsu. Acta Oceanol. Sin. 8, 197–206 (in Chinese).

Yuan, Y.R., Chen, Q., 1984. Sediments and sedimentary facies of the Abandoned Yellow River underwater delta in the South Yellow Sea. Mar. Geol. Quat. Geol. 4, 34–43 (in Chinese with English abstract).

Zhang, C.K., 2012. General report on the Jiangsu marine Survey and assessment. Science Press, Beijing.

Zhang, C.K., Zhang, D.S., Zhang, J., Wang, Z., 1999. Tidal current-induced formation-storm-induced change-tidal current-induced recovery - Interpretation of depositional dynamics of formation and evolution of radial sand ridges on the Yellow Sea seafloor. Sci. China Ser. D Earth Sci. 42, 1–12.

Zhang, L., Chen, S.L., Liu, X.X., 2014. Evolution of the abandoned Huanghe (Yellow) River delta in north Jiangsu province in 800 years. Oceanol. Limnol. Sin. 45, 626–636. doi:10.11693/hyhz20130228002

Zhang, R.S., 1984. Land-forming history of the Huanghe River delta and coastal plain of North Jiangsu. Acta Geogr. Sin. 39, 173–184 (in Chinese with English abstract).

Zhang, Y., Swift, D.J.P., Yu, Z., Jin, L., 1998. Modeling of coastal profile evolution on the abandoned delta of the Huanghe River. Mar. Geol. 145, 133–148.

Zhou, L.Y., Liu, J., Saito, Y., Zhang, Z., Chu, H., Hu, G., 2014. Coastal erosion as a major sediment supplier to continental shelves: example from the abandoned Old Huanghe (Yellow River) delta. Cont. Shelf Res. 82, 43–59. doi:10.1016/j.csr.2014.03.015

Zhu, Y.R., 1998. Numerical Simulation of Paleo-tidal current field in the subei littoral Plain area and its verification. Mar. Sci. Bull. 17, 1–7 (in Chinese with English abstract).

Zhu, Y.R., Chang, R.F., 2000. Preliminary study of the dynamic origin of the distribution pattern of bottom sediments on the continental shelves of the Bohai Sea, Yellow Sea and East China Sea. Estuar. Coast. Shelf Sci. 51, 663–680.

Zhu, Y.R., Chang, R.F., 2001. On the relationships between the radial tidal current field and the radial sand ridges in the southern Yellow Sea: a numerical simulation. Geo-Mar. Lett.21 (2), 59–65. doi: 10.1007/s003670100073.

Appendix A: Description of Acronyms Used in this Paper

AYD: the Abandoned Yellow River Delta;

OYR: the old Yellow River;

SYS: the Southern Yellow Sea.

Appendix B: Historical pictorial maps

The main aim of historical maps and the restriction of historical measuring instruments is for land allocation. Therefore, most ancient maps only show a conceptual distribution of mainland (and a few of them includes nearshore ridges). These maps neither indicate longitude or latitude nor a scale. Here, we list three historical maps. To easily discriminate the Jiangsu Coast (located between the OYR and the Yangtze River) and the OYR, the position of the OYR and the Yangtze River is especially highlighted.

Map A: This map is part of the "Provincial atlas of the great Qing Dynasty". It was drawn during 1754-1760 AD. The OYR was painted with a darker Yellow color, to discriminate the ORY from the tidal channels. With respect to the areas shown with white color bounded by black lines, we assume that it represented the subaerial region. The red circulars and quadrilaterals are named

54

after local administrations. There are three blocks emphasized as "沙" (in Chinese, meaning shoals in English) in the maps. Source: Library of Congress. Digital version is available at: https://www.loc.gov/item/2002626726/.

Map B: This map is part of the "Hai jiang yang jie xing shi tu", which was drawn up with the aim of giving an overview on the coastline, islands and ridges. Note that the orientation of this map is different from other maps. It was drawn between 1787-1801 AD. The shoreline of the Jiangsu Coast was treated as a straight line in this map. Different colors are assigned to represent the mainland, ridges and water. The most significant features of this map are the shoals, inside the green shaded regions. A series of shoals located northeast of the OYR is perpendicular to the shoreline. Shoals off the central Jiangsu Coast are parallel to the shoreline. There are also several sporadic ridges located off the southern Jiangsu Coast. Source: Library of Congress. Digital version is available at: http://www.loc.gov/item/gm71005021/.

Map C: This map is part of the "Jiang hai quan tu", drawn between 1812-1843 AD. This map was drawn as a guideline for navigation, to avoid emerged ridges, so the coast line and the major rivers of estuaries, islands and ridges along the Jiangsu Coast were labeled. The shoreline of the Jiangsu Coast was drawn as arcuate pattern. The shoals were painted with khaki color and bounded by dotted lines. The land was painted with gray colors. Source: Library of Congress. A digital version is available at: http://www.loc.gov/item/gm71005059/. Note that the scale and direction of the shoals drawn in this map are significantly different from that in the Map B.
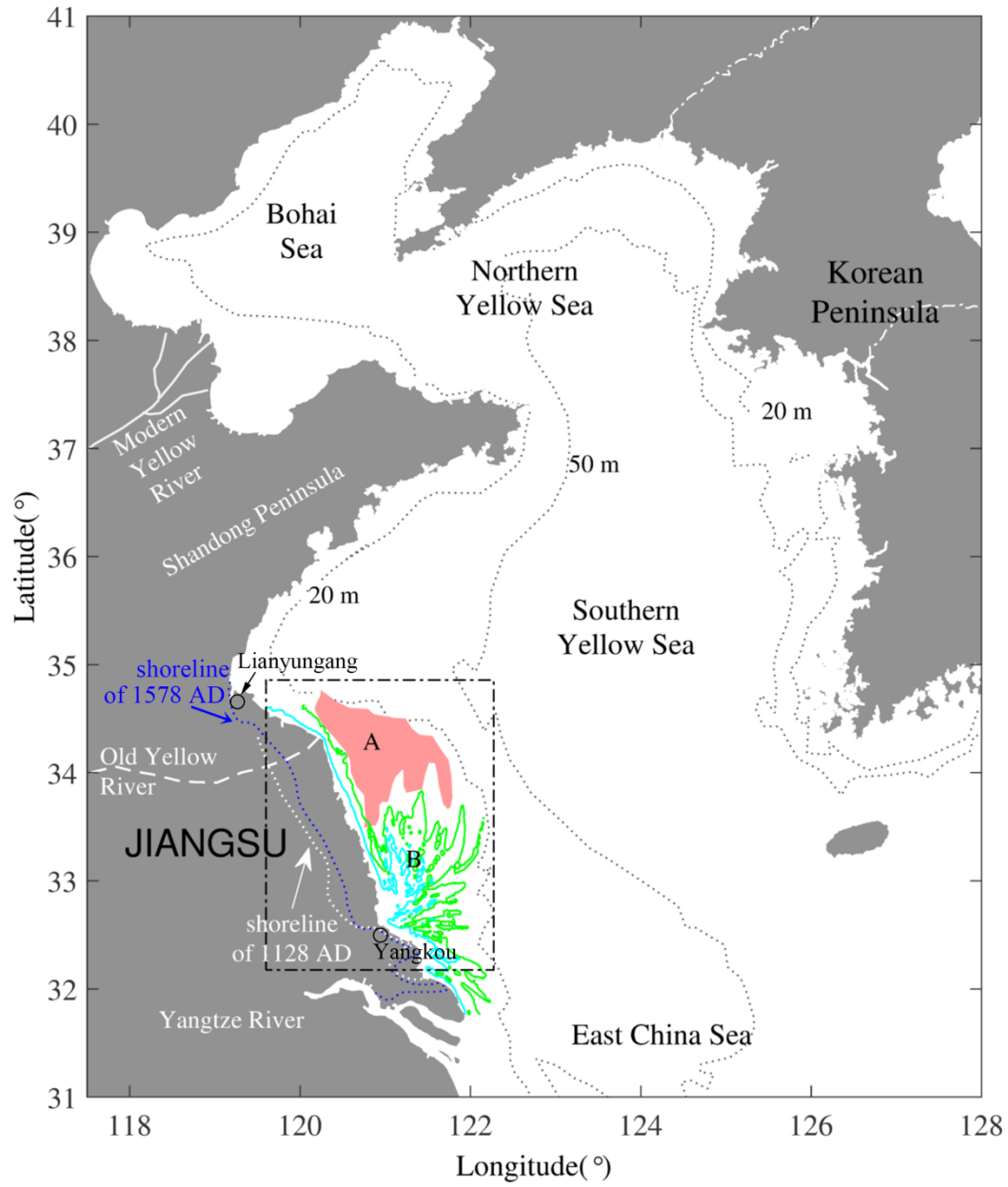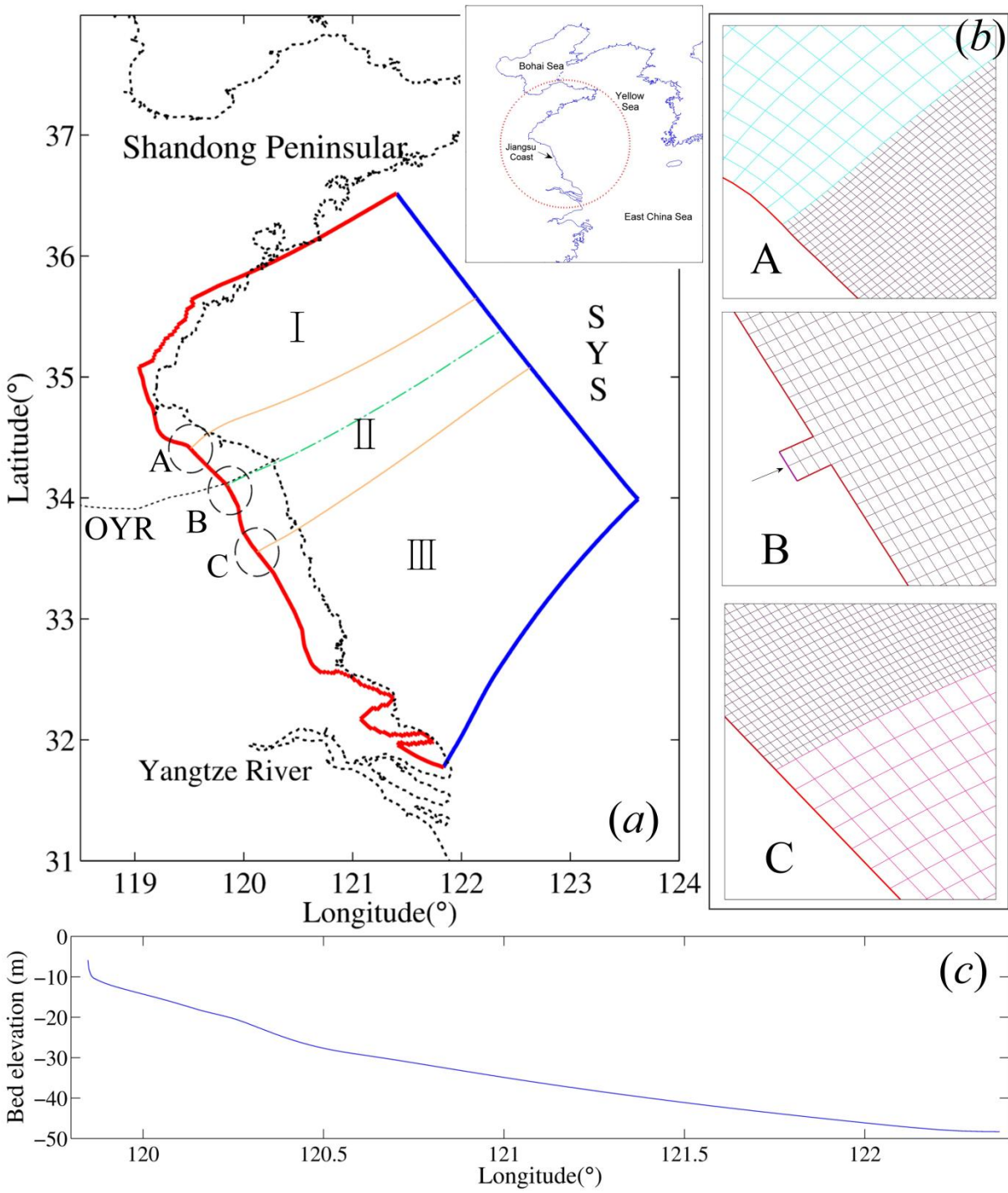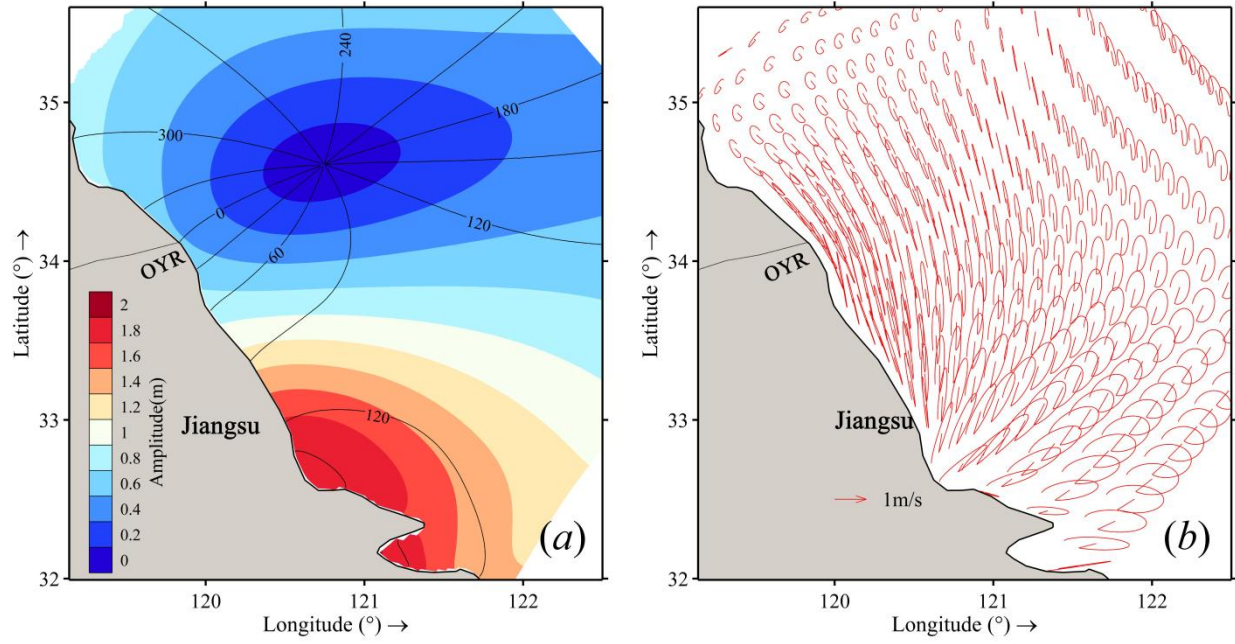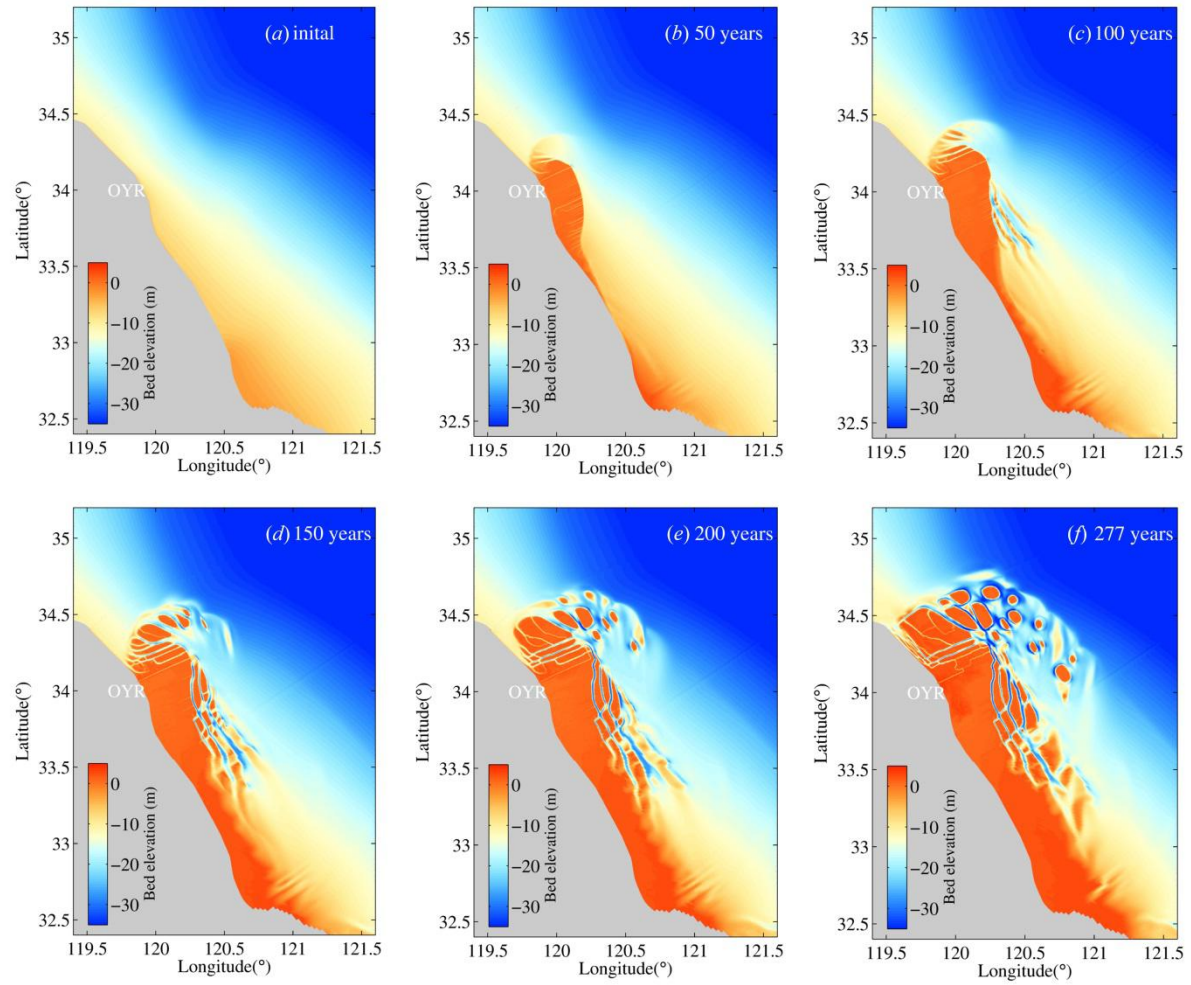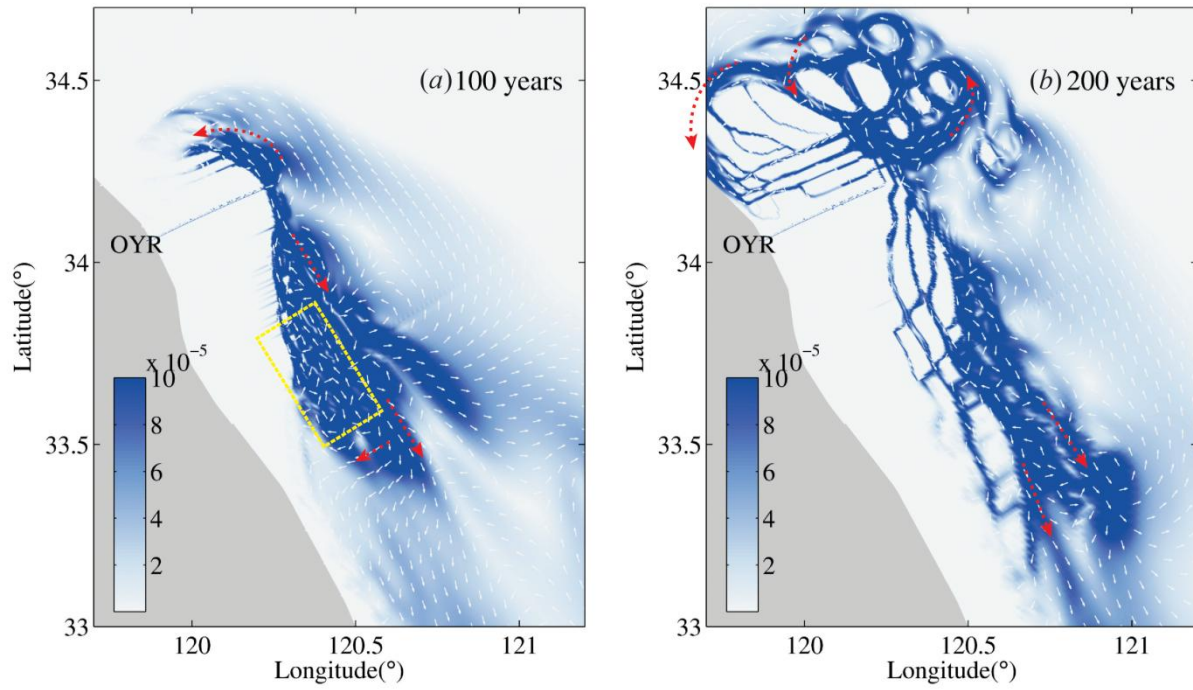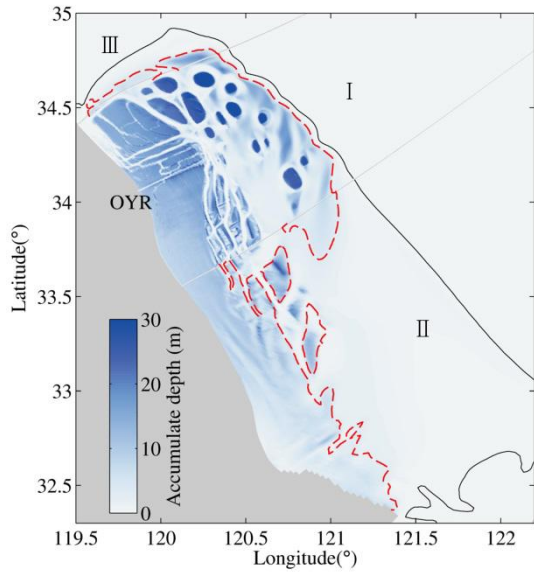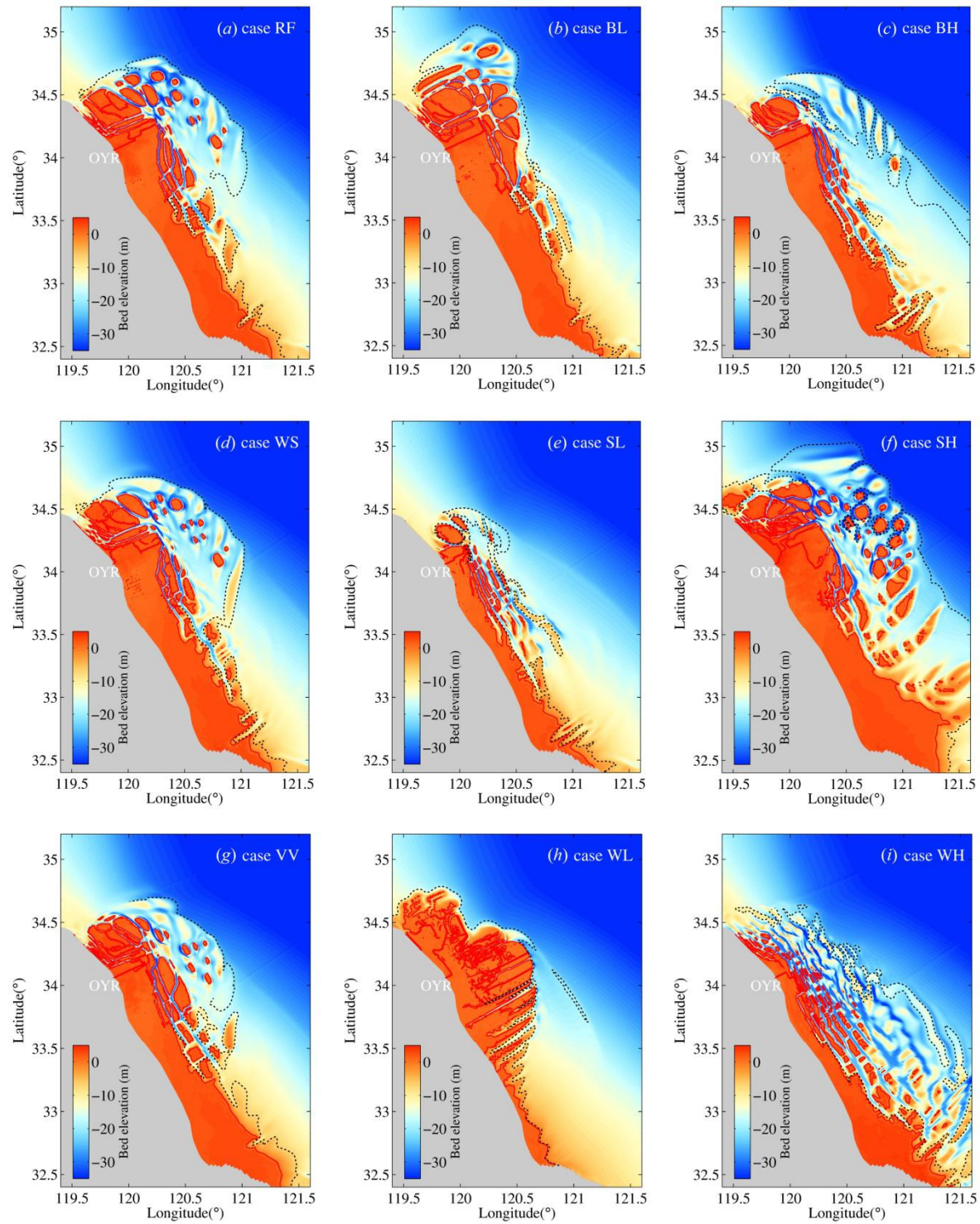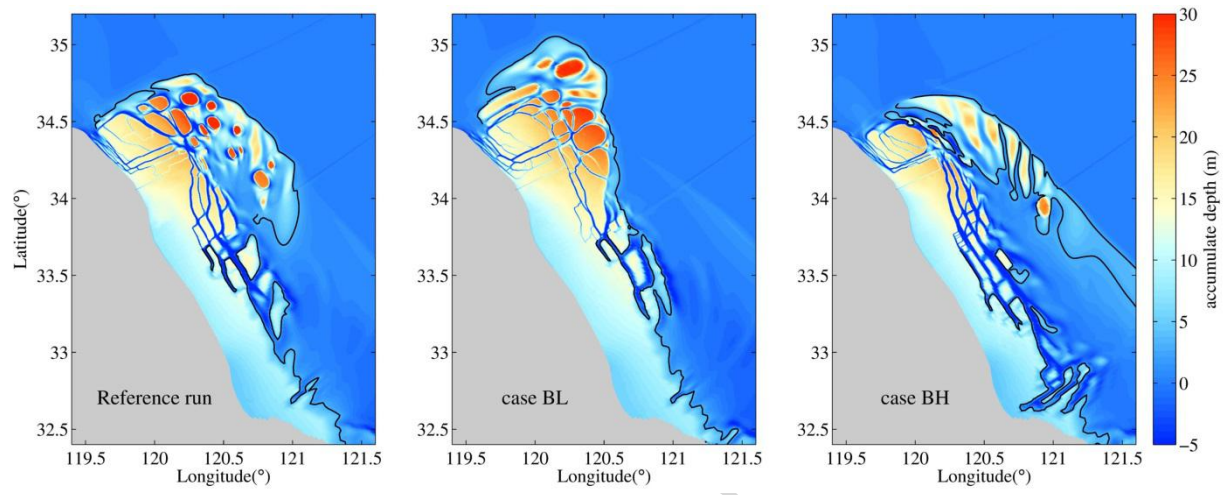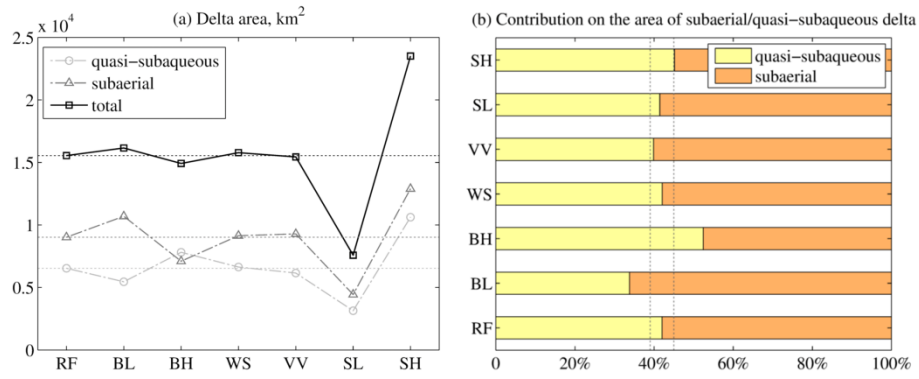
Fig. 1
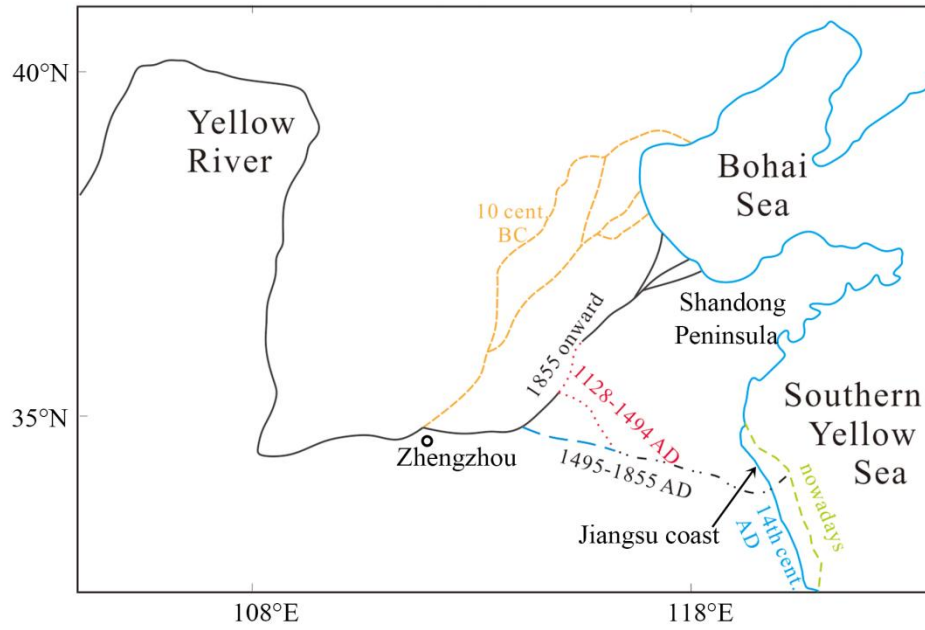
Fig. 2
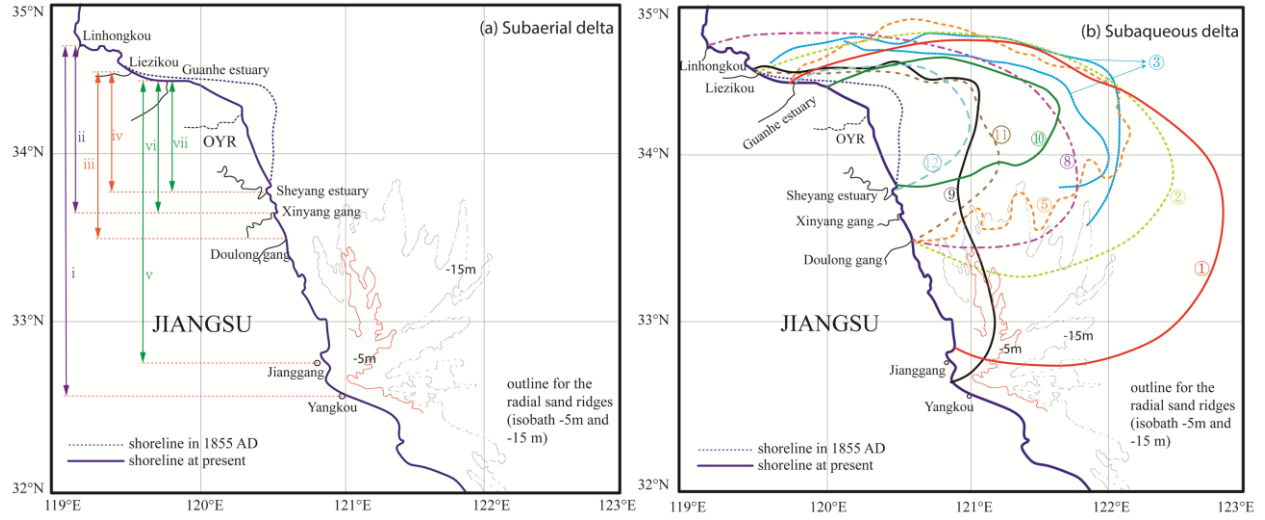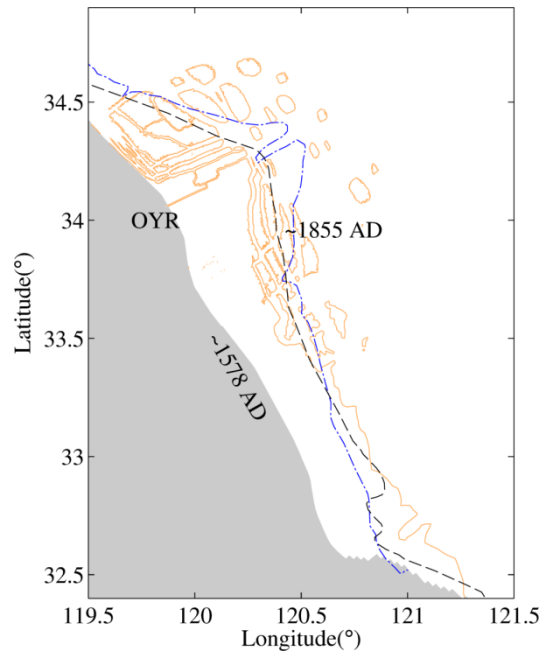
Fig. 3

Fig. 4

Fig. 5

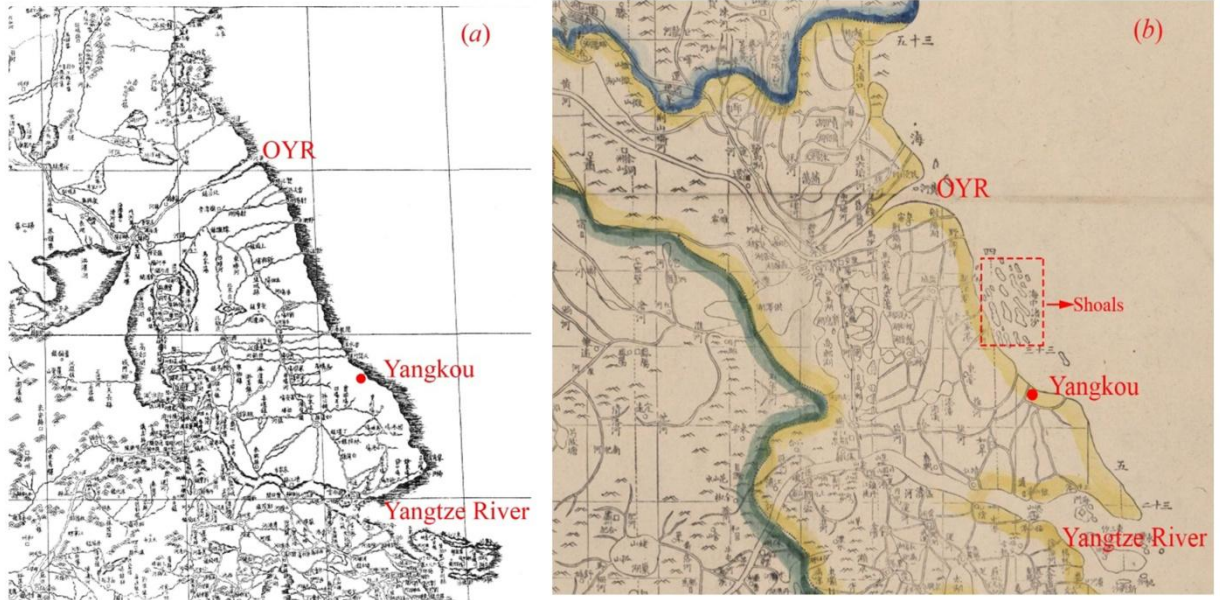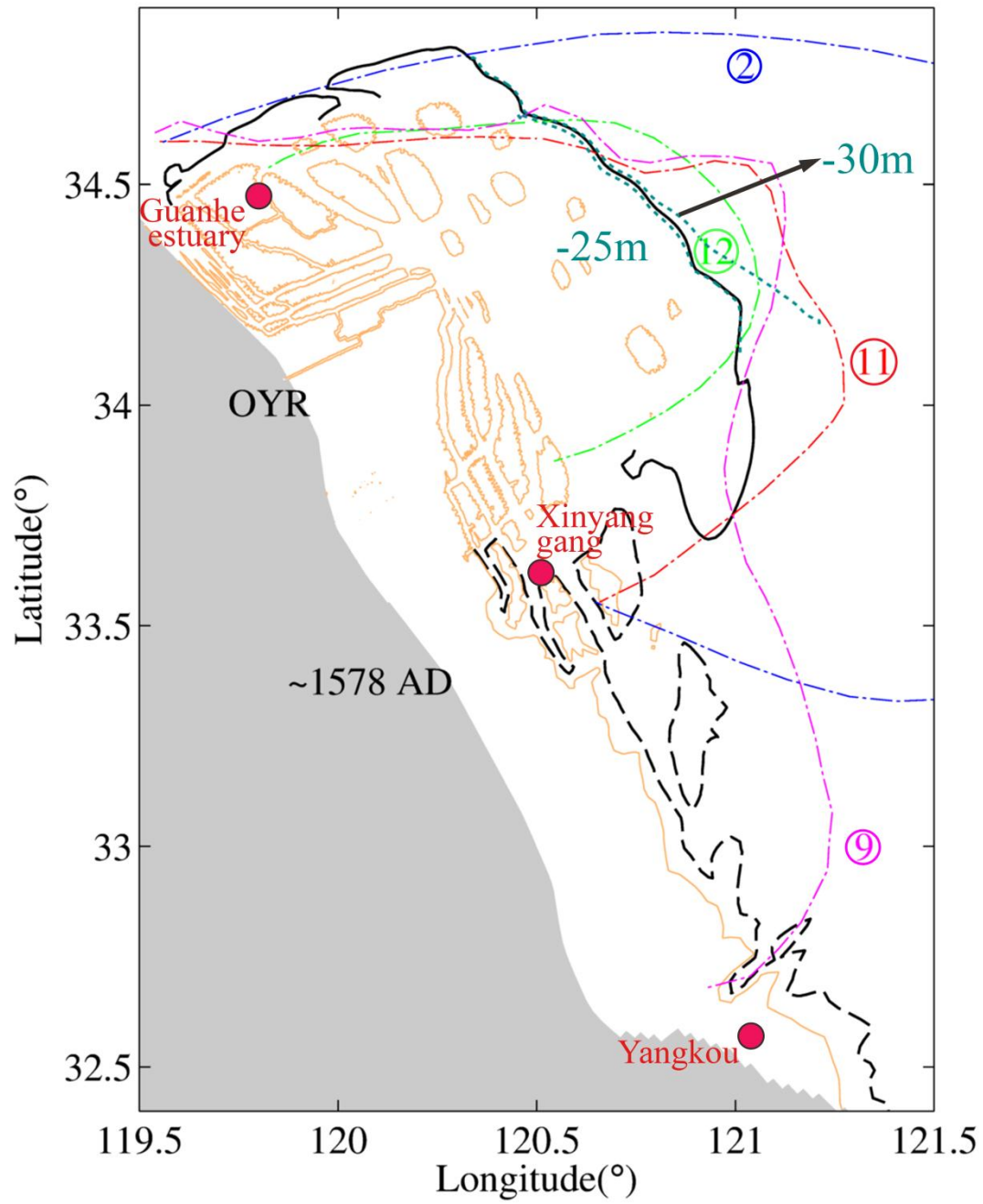Fig. 6

Fig. 7

Fig. 8

Fig. 9

Fig. 10

Fig. 11
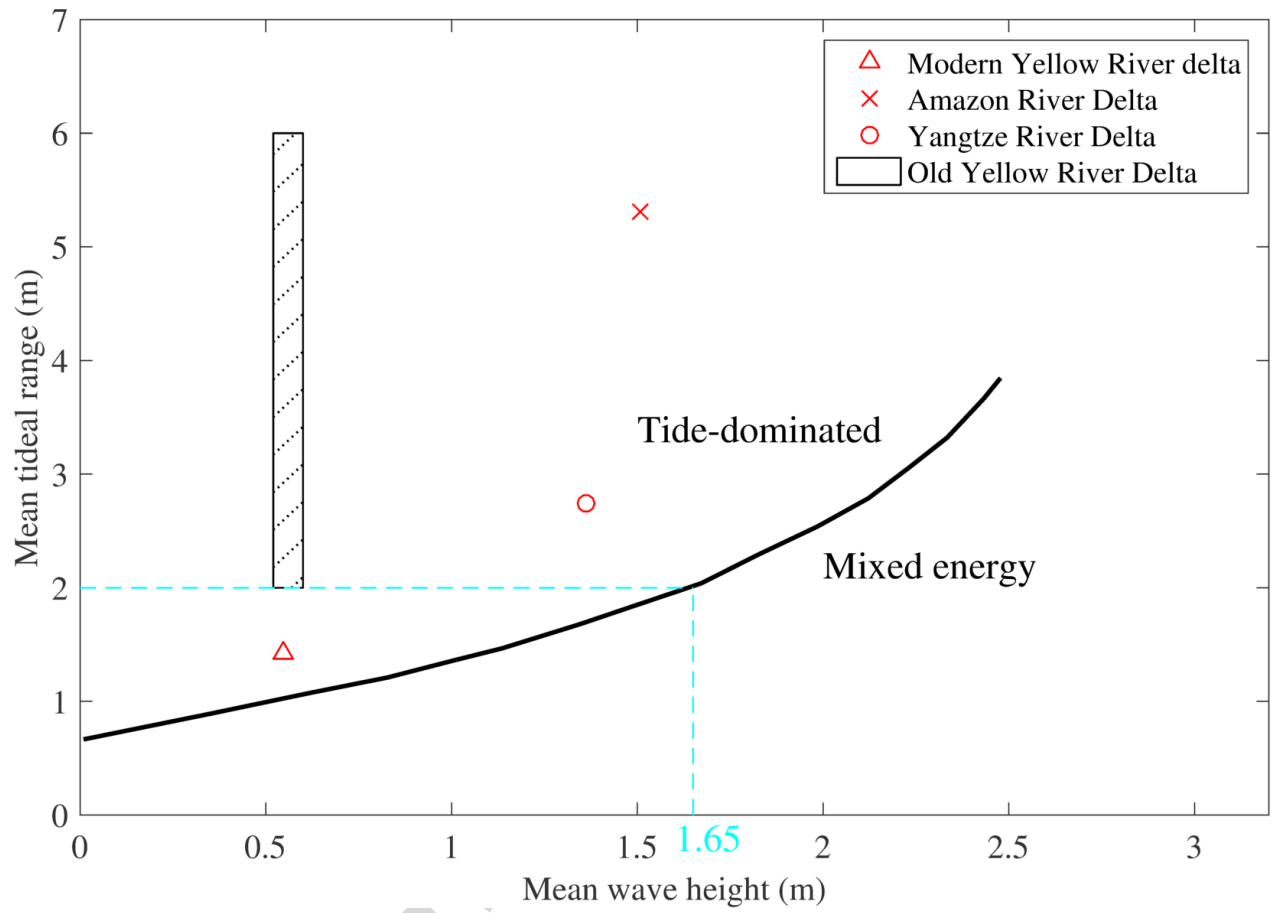
Fig. 12

Fig. 13

Fig. 14

Fig. 15

Table 1 Estimations of the size of subaerial delta of the AYD developed between 1128 – 1855 AD

No.	Length (km)	Area (km^2)	Reference	No.	Length (km)	Area (km^2)	Reference
i	~260	7100	Cheng and Xue (1997); Xue et al. (2003); Huang et al. (2005); Liu et al. (2013)	iv	120	7160[+] 4500	Zhang (1984); Ren et al. (1994)[+]
ii	173	12760	Wang (1998)	v	218	7000	Yuan and Chen (1984)
iii	~240	16000	Ye (1986); Gao et al. (1989); Li (1991)	vi	~117	-	Wan (1989)
vii	100	7000'	Chen et al. (1993)				

The number of these viewpoints is according to the geographical position of the announced northern and southern boundaries (see Figure 3a).

Table 2 Estimations of the size of subaqueous delta of the AYD developed between 1128 and 1855 AD

No.	Eastern boundary or width (km)	Northern boundary	Southern boundary	Area (km²)	Rollover Points of clinoforms	Approaches*	Reference
①	122°50′E; 50 m isobath; 220 km	~34°45′N	~32°35′N	46000	122°36′E 33°42′N	ABCD	Yuan and Chen (1984)
②	122°30′E; 30/40 m isobath	34°50′N	33°05′N	26000#	-	CD	Xu (2005)
③	121°42′E; 160 km	~34°45′N	~32°42′N	22000#	10-25 m isobath	ABCD	Liu et al. (2013)
④	25/40 m isobath; 96 km	34°32′N	~32°39′N	21000	-	ABC	Huang et al. (2005)
⑤	30/40 m isobath	34°32′N	33°33′N	19000#	30/40 m isobath	ABC	Gao et al. (1989); Li (1991)
⑥	122°E;20/30 m isobath	34°32′N	33°50′N	-	122°12′E	AB	Yu et al. (1986)
⑦	25 m isobath; 90~160 km	34°32′N	33°41′N	-	10-15 m isobath	ABCD	Xia et al. (2015)
⑧	25 m isobath	~34°45′N	~33°33′N	18000#	-	ABC	Ren and Shi (1986); Ren et al. (1994)
⑨	20 m isobath	~34°40′N	~32°39′N	9000#	-	ABC	Cheng and Xue (1997)
⑩	121°38′E; 120 km	34°32′N	33°50′N	7600	-	ABCD	Yang (1985)
⑪	17 m isobath; 72 km	34°32′N	33°50′N	6000	121°30′E	ABC	Wan (1989)
⑫	15m isobath; 25~100 km	~34°36′N	33°33′N	>6000#	15 m isobath	AB	Ye (1986)

The isobath refers to the bathymetry at present. #: the area could not be obtained from the corresponding reference but estimated by Xia et al. (2015) by means of ArcGIS. *The approaches contain (A) characteristics of topography and geomorphology, (B) sedimentary strata, (C) drill cores and (D) shallow seismic profiles.

Table 3 Applied sensitivity parameters for different scenarios.

| Parameter	Reference	Scenarios	
Initial bed slope	0.175‰	0.157‰ (BL)	0.192‰ (BH)
Sediment availability	2.4×10^8 t/y	0.8×10^8 t/y (SL)	4×10^8 t/y(SH)
c/q ratio	3/2550	4.8/1600 (WS)	
Annual variation of sediment load	no	yes (VV)[+]	
Tidal amplitude*	T	T×0.5 (WL)	T×2 (WH)

The names of scenarios are listed in parentheses, following the assigned value of uncertainties. [+]Incase VV, the sediment load changes temporally from 2 to 6 kg/m^3 and the variation of sediment concentration is corresponding to the temporal variations of shoreline extension rates illustrated in Ye (1986) and Zhang et al. (2014). "T" denotes tidal amplitude in the reference run; the tidal amplitude prescribed along the open boundaries in case WL and WH is half and twice of that in the reference run, respectively.

Map (*A*)
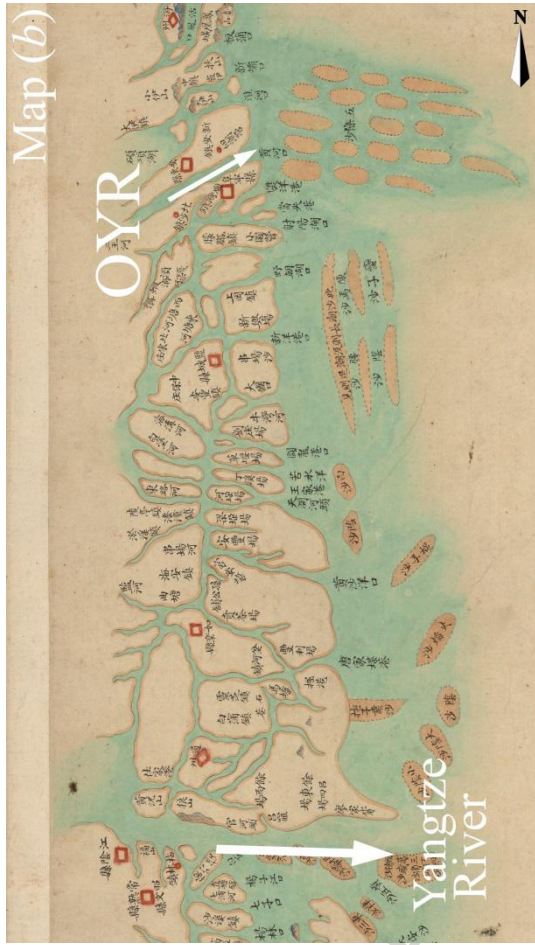
Appendix 1

Appendix 2
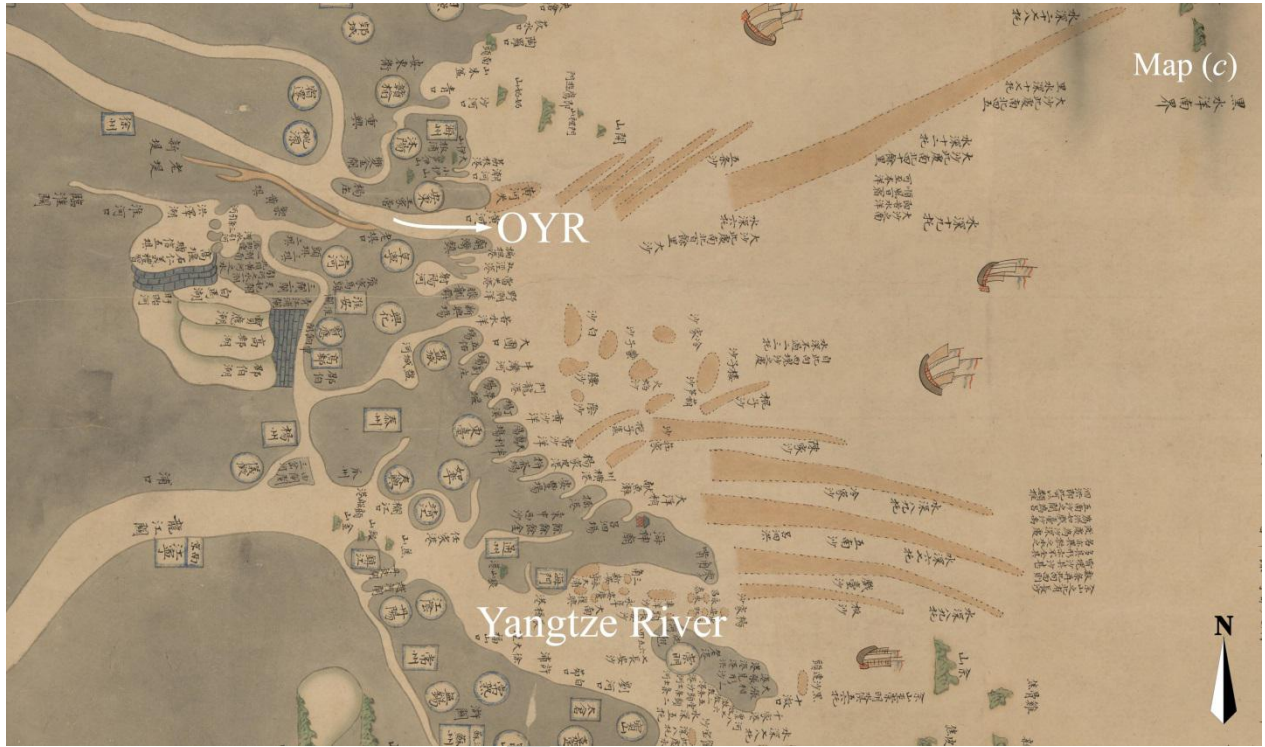
Appendix 3

Highlights

1. Provide insight into the evolution of the Abandoned Yellow River Delta (AYD) through a process-based morphodynamic-modelling approach.

2. Quantify the influence of uncertainty in model setting and initial state on the morphological evolution.

3. Simulations reproduce the AYD in good agreement with historical maps and the results of geological studies.

4. The model improves the understanding of the mechanisms underlying the evolution of the AYD.

5. The model provides relatively reliable suggestions on the spatial distribution of the AYD.